

**Technical Document 2630**
April 1994

# Rough Surface Models Implemented Within the Split-Step Parabolic Equation Algorithm

Amalia E. Barrios
*NRaD*

Kenneth H. Craig
*Radio Communications Research Unit*
*Rutherford Appleton Laboratory*
*Chilton, Didcot UK*





**Technical Document 2630**
April 1994

# Rough Surface Models Implemented Within the Split-Step Parabolic Equation Algorithm

Amalia E. Barrios
*NRaD*

Kenneth H. Craig
*Radio Communications Research Unit*
*Rutherford Appleton Laboratory*
*Chilton, Didcot UK*

**NAVAL COMMAND, CONTROL AND OCEAN SURVEILLANCE CENTER**
**RDT&E DIVISION**
**San Diego, California 92152–5001**

**K. E. EVANS, CAPT, USN**
**Commanding Officer**

**R. T. SHEARER**
**Executive Director**

## ADMINISTRATIVE INFORMATION

This work was sponsored by the Office of Naval Research, 800 N. Quincy Street, Arlington, VA, 22217, under program element 0602435N, project MP92. The work was performed during a visit by the first-named author to Rutherford Appleton Laboratory in May – June 1993.

Released by
R. A. Paulus, Head
Tropospheric Branch

Under authority of
J. H. Richter, Head
Ocean and Atmospheric
Sciences Division

## ACKNOWLEDGMENTS

The authors would like to thank Dr. Mireille Levy of RAL for very helpful discussions and for providing the rough sea surface realization used in this report. Also, many thanks to Dan Dockery of JHU/APL for his guidance in implementing the mixed transform algorithm.

One of the authors (AEB) would especially like to thank her coauthor for extending an invitation to RAL for a summer work visit and to everyone in the Radio Communications Research Unit at RAL for their hospitality. Also, thanks and appreciation to the Office of Naval Research for funding this work under the Atmospheric Effects Assessments Technology Area managed by Dr. Juergen Richter.

SM

# SUMMARY


## OBJECTIVE

Investigate and compare several rough surface models implemented within the split-step Fourier parabolic equation (PE) algorithm. Describe advantages and disadvantages of each model and their possible inclusion in current PE models.

## RESULTS

Three split-step PE rough surface models—(1) mixed transform (MT), (2) surface loss function (SLF), and (3) approximate solution (AS)—were investigated and compared with a reference waveguide model called MLAYER. The MT and SLF models are shown to agree well with MLAYER; the AS model, however, generally showed poor agreement. The MT model, though the most accurate, is the most time-consuming of the three. The AS model, the most numerically efficient, shows the poorest match to MLAYER.

In using one of these rough surface models, whether it be to model rough surface effects over ocean or variable terrain, a satisfactory compromise may be to use some form of the SLF model since it is shown to agree fairly well with MLAYER and is still fairly efficient.

# CONTENTS



## FIGURES

TABLES

# 1.0 INTRODUCTION

Recent advances in parabolic equation (PE) modeling have produced many varied techniques to account for environmental effects on radiowave propagation through the troposphere. Current PE models have been shown to successfully model range-dependent refractivity environments on propagation paths over ocean and land [1,2,3]. Most of these models deal with the simplest of cases in which a smooth, perfectly conducting ground is assumed for the boundary. For the frequency range considered in this report (0.1 to 20 GHz), finite conductivity is important at frequencies below approximately 1 GHz, and rough surface effects are a major factor at frequencies above 10 GHz.

This report will discuss several techniques in which propagation over a rough surface can be adequately modeled. Finite conductivity will also be addressed in the methods explored. The split-step Fourier (SSF) method [4] is widely accepted as being a more numerically efficient algorithm than current finite-difference techniques; therefore, this report will concentrate only on techniques implemented within the SSF method.

A description of the models and their implementations is given in Section 2.0 and results are given in Section 4.0. The rough surface SSF models are compared with a waveguide program called MLAYER, developed at NCCOSC, RDT&E Division (NRaD) by Baumgartner [5] and Pappert.* MLAYER is a rigorous model based on mode theory and uses the more accurate rough surface reflection coefficient by Miller, Brown, and Vegh [6]. In Section 3.0, MLAYER is compared favorably with experimental data in which propagation measurements were taken in the presence of 9-to-10-m/s winds, and therefore is shown to be a good reference for the SSF models.

# 2.0 ROUGH SURFACE MODELS

## 2.1 MIXED TRANSFORM ALGORITHM

The mixed transform algorithm was developed by Kuttler and Dockery [1] to model finite conductivity and rough surface boundaries within the split-step algorithm. This algorithm is now implemented in the TEMPER program developed by Dockery.** This is a mathematically rigorous approach in which the impedance boundary condition is explicitly applied at each range step. The impedance boundary condition is

$$\frac{\partial \psi(r,z)}{\partial z}\Bigg|_{z=0} + a\psi(r,0) = 0 \tag{1}$$

where

$$\alpha = ik_o \sin\vartheta_g \left(\frac{1 - R\rho_o}{1 + R\rho_o}\right) \tag{2}$$

*Pappert, R. A., "Field Strength and Path-loss in a Multilayer Tropospheric Waveguide Environment," Naval Ocean Systems Center, San Diego, California, NOSC TN 1366, October 1984. Technical Notes are working documents and do not represent an official policy statement of the Naval Ocean Systems Center, now NRaD. For further information, contact the authors.

**Dockery, G. D. "Performance of the Improved Impedance Boundary Condition Algorithm in the Tropospheric Electromagnetic Parabolic Equation Routine (TEMPER)," Applied Physics Laboratory, Laurel MD, in-house report F2B–89–U–8–015, December 1989.

$\psi(r,z)$ is the scalar component of the field, $R$ is the smooth-surface Fresnel reflection coefficient, $\vartheta_g$ is the grazing angle, and $\rho_o$ is the rough surface reduction factor defined by

$$\rho_o = e^{-\frac{g^2}{2}} I_o\left(\frac{g^2}{2}\right)$$

$$g = 2k_o\sigma_{rms}\sin\vartheta_g \tag{3}$$

In Eq. 3, $I_o$ is the modified Bessel function of zero order, $k_o$ is the free-space wavenumber, and $\sigma_{rms}$ is the standard deviation wave height determined from wind speed, $\mu$, by

$$\sigma_{rms} = 0.0051\ \mu^2 \tag{4}$$

In Eq. 4, the wind speed is specified in units of m/s, giving the standard deviation wave height in meters [7]. The formula for $\rho_o$ is taken from Miller, Brown, and Vegh [6], which gives a better estimate for fields reflected off rough surfaces and is implemented using a closed-form approximation given by CCIR Report 1008-1 [8]:

$$\rho_o \cong \frac{1}{\sqrt{3.2\chi - 2 + \sqrt{(3.2\chi)^2 - 7\chi + 9}}}$$

$$\chi = \frac{1}{2}g^2$$

When propagation is modeled over a smooth, finite conducting surface, $\rho_o$ becomes 1. After substitution of the Fresnel coefficients, using a small angle approximation, $\alpha$ becomes independent of $\vartheta_g$ and is defined by

$$\alpha \cong \frac{ik_o}{n_c};\quad \text{for vertical polarization}$$

$$\alpha \cong ik_o n_c;\quad \text{for horizontal polarization} \tag{5}$$

$$n_c = \sqrt{\varepsilon - i60\sigma\lambda}$$

The relative permittivity and conductivity are represented by $\varepsilon$ and $\sigma$, respectively, with the wavelength, $\lambda$, specified in meters.

The mixed transform algorithm incorporating the impedance boundary condition at each range step is

$$\psi(r+\Delta r,z) = e^{ik_o\Delta r\,10^{-6}M(z)}\left\{\Im_s\left[\frac{\alpha}{\alpha^2+p^2}e^{-i\frac{p^2}{2k_o}\Delta r}\Psi(r,p)\right] - \Im_c\left[\frac{p}{\alpha^2+p^2}e^{-i\frac{p^2}{2k_o}\Delta r}\Psi(r,p)\right]\right\}$$

$$\Psi(r,p) = \alpha\,\Im_s[\psi(r,z)] - p\,\Im_c[\psi(r,z)] \tag{6}$$

$$M(z) = \left(n - 1 + \frac{z}{a}\right)10^6$$

$$p = k_o\sin\vartheta$$

Here, $r$ and $z$ are the range and height variables, respectively, $n$ is the index of refraction, and $\alpha$ is the earth's radius. $\Im_s$ and $\Im_c$ represent Fourier sine and cosine transforms, respectively. A term which accounts for surface wave effects has been omitted in Eq. 6. For our frequency range of interest, this additional term has very little effect.

To model rough surface effects, it is necessary to determine the grazing angle at each range for substitution into the parameter $\alpha$. A spectral estimation procedure (FFT with Hanning window) must be performed on a smooth surface, horizontal polarization solution, and the grazing angles are then used to produce the rough surface solution. As stated by Dockery (*op. cit.*), using a smooth surface and horizontal polarization solution to determine the grazing angles may cause some error in the final result for rough surfaces, but such error is considered to be small. A more sophisticated spectral estimation procedure is implemented within TEMPER and is based on the Multiple Unknown Signal Identification and Classification (MUSIC) algorithm. However, the more standard procedure used here of applying FFTs is believed to be sufficient. Figure 1 shows a comparison of grazing angle vs. range determined from TEMPER and from an 8-pt and 16-pt FFT spectral estimation. That is, only the fields in the lower 8 bins ($8*\Delta z$) and 16 bins, respectively, were used to determine the grazing angle, with the FFTs performed on an array zero-padded to 512 points. The refractivity is a homogeneous 45.7-meter surface duct, with the antenna height at 22.9 meters and frequency at 10 GHz.

A note should be made here on the use of both sine and cosine transforms in this method. When smooth surface and horizontal polarization are modeled (and it is assumed that infinite conductivity is a good approximation for all our radar frequencies of interest), only sine transforms need be used. Sine and cosine transforms are required only when vertical polarization with finite conductivity, and rough surface effects, are modeled.

## 2.2 SURFACE LOSS FUNCTION

The surface loss function model was originally developed by Moore-Head, Jobst, and Holmes [9] for acoustic underwater waves incident on rough boundaries. The model is based on a surface loss-vs.-angle description of the boundary implemented within the split-step Fourier algorithm. This model is a semiempirical model since it applies an angle-dependent surface loss function to the field in a layer near the ocean surface. Therefore, the model is not a result of rigorous mathematical derivation, but instead relies on attenuating the field near the surface by something physically meaningful.

The field is separated into three height regions. One is a surface layer of height $d$ in which the field is assumed to have a strong interaction with the ocean surface. A second layer, also of height $d$, is a transition layer, and the third layer corresponds to all heights greater than $2d$. The field, in terms of the loss function, $L(p)$, is formulated below:

$$\psi(r+\Delta r,z) = \Im^{-1}\left\{L(p)\,\Im\left[w(z)\psi_1(r+\Delta r,z)\right]\right\} + \left[1-w(z)\right]\psi_1(r+\Delta r,z) \quad for\ z \le 2d$$

$$\psi(r+\Delta r,z) = \psi_1(r+\Delta r,z) \qquad for\ z > 2d$$

where $\psi_1(r+\Delta r,z)$ is the field obtained by the smooth earth split-step algorithm:

$$\psi_1(r+\Delta r,z) = e^{ik_o\Delta r\,10^{-6}M(z)}\,\Im^{-1}\left\{e^{-i\frac{p^2}{2k_o}\Delta r}\left[\psi_1(r,z)\right]\right\}$$

The loss function, $L(p)$, is defined in terms of a surface loss-vs.-angle function, $SL(\vartheta)$, in dB, where $SL(\vartheta)$ is the loss of the field in dB due to one surface reflection at grazing angle $\vartheta$. The loss function is defined as

$$L(p) = L(k_o \sin\vartheta) = 10^{-\frac{1}{20}\left(\frac{SL(\vartheta)}{N}\right)}$$

Here, $N$ is the number of range steps in which the incident ray at angle $\vartheta$ remains in the surface and transition layers and is determined by geometry

$$R_s = \frac{2d}{\tan\vartheta} \; ; N = \frac{R_s}{\Delta r}$$

The loss due to each surface reflection is effectively "smeared" so that over the range $R_s$, the portion of the field below a height of $2d$ is reduced by $SL(\vartheta)$. Here, $SL(\vartheta)$ is a function of the rough surface reflection coefficient reduction factor, $\rho_o$, and is given by $-20*\log\rho_o$. The loss function, $L(p)$ now becomes

$$L(p) = \rho_o^{\frac{1}{N}}$$

The weighting function, $w(z)$, is the same as that used by Moore-Head, Jobst, and Holmes (*op. cit.*), and is applied in the transition layer to smooth the field in order to avoid introducing discontinuities from the surface to the upper layer. $w(z)$ is defined below:

$$w(z) = \begin{cases} 1 & \text{for } z \le d \\ \cos\left[\dfrac{\pi(z-d)}{2d}\right] & \text{for } d < z \le 2d \\ 0 & \text{for } z \ge 2d \end{cases}$$

Because of this particular choice for $w(z)$, the range over which a ray remains in the surface and transition layers is redefined:

$$R_s = \frac{2d_{eff}}{\tan\vartheta_g} \; ; \text{where} \int_o^{2d} w(z)dz = d_{eff} = d + \frac{2d}{\pi}$$

The formula for $d_{eff}$ differs here from that given in Ref. 8, which is incorrect. Unlike the first model, in which the grazing angle must be determined at each range step for substitution into $\rho_o$, the angles used for substitution in $L(p)$ are the angles defined by the PE transform variable taken only over the number of bins corresponding to the surface layer height.

An attractive feature of this method is that since the attenuation due to a rough surface is contained within the loss function $L(p)$, when rough surface effects are modeled by the method just described, only sine transforms are required as in the smooth earth split-step algorithm. Modeling vertical polarization and finite conductivity will be addressed in Section 5.0.

## 2.3 APPROXIMATE SOLUTION

The approximate solution model was developed by Prof. Fred Tappert of the University of Miami and is based on Monte Carlo techniques to create a realization of the random sea surface.

Very little documentation exists on this method, and the implementation described here has been taken from actual source code written by Prof. Tappert while working under contract at NOSC during the summer of 1990.

The rough surface boundary condition is approximated by a Taylor series expansion about $z$=0, resulting in the impedance boundary condition:

$$\psi(\eta(r),r) = 0 \approx \psi(0,r) + \eta(r)\frac{\partial\psi}{\partial z}\bigg|_{z=0} \tag{7}$$

The range-dependent surface displacement is represented by $\eta(r)$ and is considered as a random quantity. The impedance boundary condition can be formally put into the PE to yield a new equation in which a new index of refraction is defined.* The refractivity term in the smooth earth split-step algorithm is now replaced with

$$10^{-6}M(z) - \frac{\eta(r)}{2k_o^2}\delta''(z) \tag{8}$$

In Eq. 8, $\delta''(z)$ is the second derivative of the delta function, and numerically, can be realized by the function

$$\delta''(z) = \frac{4}{\sqrt{\pi}\ L_s^3}\ e^{-\frac{z^2}{L_s^2}}$$

where $L_s$ is the surface mixing length and is determined at each range step by summing the *p-space field given by*

$$L_s = \left[\frac{\sum_{i=0}^{N-1}\left(x_i^2 + y_i^2\right)}{\sum_{i=0}^{N-1}(i\Delta p)^2\left(x_i^2 + y_i^2\right)}\right]^{\frac{1}{2}} \tag{9}$$

$$\Delta p = \frac{\pi}{z_{\max}}$$

Here, $z_{max}$ is the maximum height of the calculation domain, $N$ is the transform size, and the $x_i s$ and $y_i s$ are the real and imaginary parts of the field, respectively. It is worth noting that in Eq. 9, $\delta''(z)$ rapidly falls to zero as the height, $z$, increases, making the additional rough surface term in Eq. 8 negligible at higher heights. This is similar in concept to the method described in Section 2.2.

The Toba spectrum is used to describe the sea surface:

$$S(K) = \frac{\gamma\sigma_{rms}^2\ L_c}{\left[1 + (KL_c)^2\right]^{\frac{5}{4}}}$$

*W. Li, "Rough Sea-Surface Forward Scattering," draft of Master's thesis, University of Miami, July 1993.

where the normalization coefficient is

$$\gamma = \frac{\Gamma\left(\frac{5}{4}\right)}{\Gamma\left(\frac{1}{2}\right)\Gamma\left(\frac{3}{4}\right)}$$

The spectrum is randomized according to the procedure

$$S_i = [-2 \ln(a_i)\, \Delta K\, S(i\Delta K)]^{\frac{1}{2}} \cos(2\pi b_i) \quad \text{for } i = 0, 1, \ldots, N-1$$

$$\Delta K = \frac{2\pi}{N\Delta r}$$

in which the $a_i$s and $b_i$s are random numbers uniformly distributed between 0 and 1. Next, a cosine FFT is performed on the $S_i$s and the resulting series is used for $\eta(r)$. Only the real portion of the randomized spectrum is considered here for the sea surface realization.

As in the surface loss function method, only sine transforms are used here to model rough surface effects. Vertical polarization and finite conductivity will be addressed in Section 5.0.

## 3.0 REFERENCE MODEL

In order to conduct an investigative study of the validity of the rough surface models discussed in Section 2.0, they must be compared against a suitable reference. This section will establish that the waveguide program MLAYER is such a reference model. MLAYER is compared with experimental radio data that were measured in the presence of high wind speeds. Propagation measurements were taken in the 1–40 GHz frequency range between the Greek islands of Naxos and Mykonos during 1972 [10]. Meteorological measurements were routinely taken at the meteorological station of the Greek Weather Service on Naxos. The transmitters were located on Naxos, with receiving terminals on Mykonos. Propagation measurements were made during the months of February, April, August, and November, lasting approximately two weeks each. The transmitting and receiving terminals were separated by a distance of 35.2 km. Only those time periods consisting of high wind speeds, in this case November 7 and 8 and August 8–13, are considered here. Tables 1 and 2 give the air temperature, sea temperature, humidity, and wind speeds measured during these periods.

Table 1. Meteorological measurements for November 7 and 8, 1972.

| Day | Hour | Air Temp, C° | Sea Temp, C° | Relative Humidity | Wind Speed, m/s |
|---|---|---|---|---|---|
| 7 | 10 | 18.0 | 18.0 | 80 | 5.0 |
| 7 | 11 | 18.0 | 18.0 | 82 | 5.0 |
| 7 | 12 | 18.0 | 18.0 | 81 | 4.0 |
| 7 | 13 | 19.0 | 18.0 | 72 | 5.0 |
| 7 | 14 | 18.0 | 18.0 | 72 | 8.0 |
| 7 | 15 | 18.0 | 18.0 | 72 | 9.0 |
| 7 | 16 | 18.0 | 18.0 | 72 | 10.0 |
| 7 | 17 | 17.0 | 18.0 | 74 | 10.0 |

(Contd)

Table 1. Continued.

| Day | Hour | Air Temp, C° | Sea Temp, C° | Relative Humidity | Wind Speed, m/s |
|---|---|---|---|---|---|
| 7 | 18 | 17.0 | 18.0 | 75 | 10.0 |
| 7 | 19 | 17.0 | 17.0 | 77 | 9.0 |
| 7 | 20 | 17.0 | 17.0 | 80 | 9.0 |
| 7 | 21 | 17.0 | 17.0 | 80 | 9.0 |
| 7 | 22 | 17.0 | 17.0 | 70 | 10.0 |
| 7 | 23 | 17.0 | 17.0 | 70 | 10.0 |
| 8 | 00 | 17.0 | 17.0 | 67 | 10.0 |
| 8 | 01 | 17.0 | 17.0 | 69 | 10.0 |
| 8 | 02 | 16.0 | 17.0 | 68 | 9.0 |
| 8 | 03 | 16.0 | 17.0 | 68 | 8.0 |
| 8 | 04 | 16.0 | 16.0 | 67 | 9.0 |
| 8 | 05 | 16.0 | 16.0 | 60 | 9.0 |
| 8 | 06 | 16.0 | 16.0 | 65 | 10.0 |
| 8 | 07 | 16.0 | 16.0 | 66 | 10.0 |
| 8 | 08 | 16.0 | 16.0 | 65 | 8.0 |
| 8 | 09 | 16.0 | 17.0 | 64 | 8.0 |
| 8 | 10 | 17.0 | 17.0 | 65 | 10.0 |
| 8 | 11 | 17.0 | 17.0 | 65 | 10.0 |
| 8 | 12 | 17.0 | 17.0 | 65 | 10.0 |
| 8 | 13 | 17.0 | 17.0 | 65 | 9.0 |
| 8 | 14 | 17.0 | 17.0 | 62 | 9.0 |
| 8 | 15 | 17.0 | 17.0 | 64 | 10.0 |
| 8 | 16 | 17.0 | 17.0 | 65 | 10.0 |
| 8 | 17 | 17.0 | 17.0 | 67 | 9.0 |
| 8 | 18 | 15.0 | 17.0 | 69 | 10.0 |
| 8 | 19 | 16.0 | 17.0 | 72 | 10.0 |
| 8 | 20 | 16.0 | 17.0 | 71 | 10.0 |
| 8 | 21 | 16.0 | 17.0 | 70 | 8.0 |
| 8 | 22 | 16.0 | 17.0 | 70 | 7.0 |
| 8 | 23 | 15.0 | 17.0 | 70 | 5.0 |

Table 2. Meteorological measurements for August 8–13, 1972.

| Day | Hour | Air Temp, C° | Sea Temp, C° | Relative Humidity | Wind Speed, m/s |
|---|---|---|---|---|---|
| 8 | 20 | 20.0 | 26.1 | 94 | 10.0 |
| 9 | 02 | 25.0 | 26.1 | 78 | 10.0 |
| 9 | 08 | 25.0 | 26.0 | 78 | 10.0 |
| 9 | 14 | 25.0 | 25.9 | 78 | 10.0 |
| 9 | 20 | 26.0 | 25.7 | 79 | 10.0 |
| 10 | 02 | 26.0 | 25.5 | 79 | 12.5 |

(Contd)

Table 2. Continued.

| Day | Hour | Air Temp, C° | Sea Temp, C° | Relative Humidity | Wind Speed, m/s |
|---|---|---|---|---|---|
| 10 | 08 | 26.0 | 25.3 | 74 | 10.0 |
| 10 | 14 | 28.0 | 25.1 | 70 | 10.0 |
| 10 | 20 | 26.0 | 24.9 | 74 | 12.5 |
| 11 | 02 | 26.0 | 24.7 | 74 | 12.5 |
| 11 | 08 | 25.0 | 24.6 | 78 | 10.0 |
| 11 | 14 | 27.0 | 24.5 | 74 | 10.0 |
| 11 | 20 | 29.0 | 24.5 | 55 | 15.0 |
| 12 | 02 | 26.0 | 24.5 | 61 | 10.0 |
| 12 | 08 | 26.0 | 24.5 | 74 | 10.0 |
| 12 | 14 | 27.0 | 24.5 | 74 | 15.0 |
| 12 | 20 | 26.0 | 24.5 | 74 | 10.0 |
| 13 | 02 | 26.0 | 24.5 | 74 | 10.0 |
| 13 | 08 | 25.0 | 24.5 | 78 | 15.0 |
| 13 | 14 | 26.0 | 24.5 | 74 | 10.0 |

Methods outlined in Ref. 10 were used to create an evaporation duct profile from each set of bulk measurements. MLAYER was then run using each of these profiles to obtain a loss value at the receiving terminals. Since high-frequency signals are greatly affected by a rough ocean surface, only those propagation measurements taken at frequencies of 37.44 GHz (Ka band) and 17.96 GHz (Ku band) are compared with predicted values given by MLAYER. At these frequencies, there is some added attenuation due to atmospheric absorption; therefore, this additional loss (4–7 dB) was subtracted from the measured values to give a fair comparison with the absorption-free loss values given by MLAYER. At Ka band, the transmitter height is 5.1 meters above mean sea level (msl), and the two receiver heights are at 3.6 meters and 8.6 meters. At Ku band, the transmitter height is 4.5 meters above msl, and the three receiver heights are at 4.3 meters, 9.5 meters, and 17.8 meters.

Figures 2 and 3 show absorption-free propagation loss vs. time for the low and high receiver heights, respectively, at Ka band for November 7–9. Propagation loss values from MLAYER for both a rough and smooth surface are shown in the figures. For reference, the free-space and diffraction loss levels are also shown . The diffraction fields were calculated based on a standard 4/3 effective- earth-radius atmosphere. In figure 2, the predicted loss values for an assumed smooth surface show considerably higher signal levels than were measured. However, for a rough surface, there is very good agreement between MLAYER and the measured loss values. For the receiver height at 8.6 meters (figure 3), the predicted rough surface loss values are approximately 5 to 10 dB lower than observations, but still show more attenuation than the smooth surface loss values.

Figures 4, 5, and 6 show similar comparisons at Ku band for receiver heights at 4.3 meters, 9.5 meters, and 17.8 meters respectively, for August 8–13. Between August 9 and 10, relatively high signal levels were measured. This may be due to some elevated trapping layers that were not measured or accounted for. Only during the month of November were radiosondes launched midway between Naxos and Mykonos to measure elevated refractive layers. For low and middle receiver heights, good agreement is shown between the MLAYER rough surface loss values and

observations. For the receiver height at 17.8 meters, there is very little difference between the rough and smooth surface predicted loss values, but both are still within a few decibels of the upper loss values measured. The discrepancy between the smooth surface loss and observations becomes less pronounced as the receiver height increases, indicating that the field is most affected only near the surface. This is consistent with the methods by Tappert [4] and Moore-Head, Jobst, and Holmes [9], in which the field is only attenuated within a very small layer near the surface.

As a second validity check for MLAYER, a height/range profile was created for one realization of a random sea surface using the Pierson–Moskowitz ocean wave spectrum [12]. This profile was used as input to TPEM (Terrain Parabolic Equation Model) [3], which models radiowave propagation over variable terrain. In the following cases, and in the comparisons to be given in Section 4.0, only two homogeneous refractivity environments will be used—a strongly trapping 45.7-meter surface duct and a 24-meter evaporation duct. The height vs. M-unit profiles are listed in tables 3 and 4 for the surface duct and evaporation duct, respectively. Only frequencies at 10 GHz and 20 GHz are considered. In the following coverage diagrams, the msl has been artificially raised and is represented by a second horizontal line slightly above the x-axis. All refractivity profiles are relative to this msl, and all sea-surface realizations were created using a wind speed of 20 m/s.

Table 3. Height/refractivity profile for 45.7-meter surface duct.

| Height, m | M-unit |
|---|---|
| 0. | 350. |
| 45.7 | 334.68 |
| 1524 | 506.71 |

Table 4. Height/refractivity profile for 24-meter evaporation duct.

| Height, m | M-unit |
|---|---|
| 0.0 | 0.0 |
| .135 | –20.4 |
| .223 | –21.89 |
| .368 | –23.37 |
| .607 | –24.84 |
| 1.000 | –26.29 |
| 1.649 | –27.71 |
| 2.718 | –29.08 |
| 4.482 | –30.35 |
| 7.389 | –31.49 |
| 12.182 | –32.39 |
| 20.086 | –32.90 |
| 24.000 | –32.95 |
| 33.115 | –32.78 |
| 54.598 | –31.59 |
| 90.017 | –28.66 |
| 148.413 | –22.86 |

Figure 7 shows a coverage diagram from TPEM for a frequency of 10 GHz and a 45.7-meter surface duct. A height vs. loss plot comparing MLAYER and TPEM at a range of 200 km is shown in figure 8. The rough surface result given by MLAYER agrees very well with that given by TPEM. For reference, the smooth surface result is shown to indicate the substantial amount of attenuation possible at this frequency and wind speed. While there may not be a point-by-point match between MLAYER and TPEM, it should be understood that this is just one random realization of the sea surface. A more appropriate comparison would have been to create perhaps 100 or 1000 sea surface realizations and corresponding TPEM results. The TPEM results, after averaging, could then be compared with MLAYER. This was not done here because of the tediousness of the task.

A coverage diagram from TPEM for a frequency of 20 GHz and the corresponding height vs. loss plot comparing MLAYER at a range of 100 km are shown in figures 9 and 10, respectively. Here again, there is good agreement between TPEM and the rough surface result from MLAYER. Similar coverage diagrams and height vs. loss plots are shown in figures 11 and 12 for the 24-meter evaporation duct at 10 GHz, and in figures 13 and 14 for the same evaporation duct at 20 GHz. For this environment, MLAYER shows very good agreement as it did for the surface duct.

With a reference model established that can model propagation over a rough sea surface up to 20 m/s wind speeds, we now proceed to compare the split-step PE models discussed in Section 2.0.

## 4.0 RESULTS

All the following comparisons will be displayed on height vs. propagation loss (in decibels) plots. Only the following combinations of frequency, wind speed, and receiver ranges will be considered:

1. 10 GHz at wind speed of 10 m/s, receiver range at 200 km
2. 10 GHz at wind speed of 20 m/s, receiver range at 200 km
3. 20 GHz at wind speed of 10 m/s, receiver range at 200 km
4. 20 GHz at wind speed of 20 m/s, receiver range at 100 km

Comparisons will be made for each of the above cases using both the surface duct and evaporation duct environments given in tables 3 and 4. The surface loss function (SLF) and the approximate solution (AS) models will be compared with MLAYER using horizontal polarization and perfect conductivity. Since the mixed transform (MT) algorithm was initially developed to accurately model vertical polarization and finite conductivity, results from this method will be compared with MLAYER using vertical polarization. Permittivity and conductivity values for sea water at the frequencies listed are taken from CCIR curves. More will be said about modeling vertical polarization for the SLF and AS models in Section 5.0.

Figure 15 shows the smooth surface MT and MLAYER results for the surface duct environment at 10 GHz and at a range of 200 km. The horizontal polarization result from MLAYER is also shown for comparison. At this rather long range, the vertical polarization loss values from MLAYER show approximately 5 dB more attenuation than that for horizontal polarization—and

this is accurately accounted for by the MT model. The AS and SLF models, compared with MLAYER for a wind speed of 10 m/s, are shown in figure 16a and the corresponding comparison for vertical polarization using the MT model is shown in figure 16b. For this case, the SLF model shows excellent agreement with MLAYER, with the AS model differing by as much as 25 dB. In figure 16b, the MT model shows a good match to MLAYER near the surface, but above a height of 40 meters, this method does not attenuate the field as strongly.

For the evaporation duct environment, a comparison of the smooth surface MT result and MLAYER for vertical polarization is shown in figure 17. Again, there is excellent agreement with MLAYER. Comparisons between the three models and MLAYER for a wind speed of 10 m/s are shown in figures 18a and 18b. For this case, all three models performed somewhat poorly, with the AS model differing from MLAYER by as much as 30 dB for some heights. It is surprising that the SLF and MT models did not equal their performance in figures 16a and 16b—the only difference here being the refractivity environment. A possible explanation for the large discrepancies shown in figures 18a and 18b will be given in Section 5.0.

Similar comparisons for a 20-m/s wind speed and a 200-km receiver range are shown in figures 19a and 19b and figures 20a and 20b for the surface duct and evaporation duct environments, respectively. In figure 19a, the SLF model shows the best agreement with MLAYER, while the AS model shows the largest difference—roughly 60 dB. The MT model (figure 19b) underestimates the losses by approximately 15 dB. For the evaporation duct environment, the MT model shows very good agreement with MLAYER, with the AS model off by approximately 10 dB, and the SLF model showing the poorest agreement (figures 20a and 20b).

At 20 GHz, for a smooth surface and vertical polarization, the MT model shows excellent agreement with MLAYER for the surface duct environment (figure 21). For a 10-m/s wind speed and a 200-km receiver range, the SLF model shows the best comparison (figure 22a), with the AS model differing by 35–40 dB. In figure 22b the MT model differs from MLAYER by about 8 dB. For the evaporation duct environment, the MT model again compares very well with MLAYER for the smooth surface case (figure 23). In figure 24a, for a wind speed of 10 m/s, the SLF model underestimates the loss by 5–10 dB, whereas the AS model underestimates the loss by approximately 30 dB at the lower heights. In figure 24b, there is excellent agreement between the MT model and MLAYER.

Figures 25a and 25b show comparisons between the rough surface models and MLAYER using the surface duct environment at a wind speed of 20 m/s and a receiver range of 100 km for horizontal and vertical polarization, respectively. The SLF model shows the best agreement, whereas the AS model differs by approximately 45 dB for some heights. In figure 25b, the MT model underestimates the losses at some heights by approximately 25 dB. Similar comparisons are shown for the evaporation duct environment in figure 26a (horizontal polarization) and figure 26b (vertical polarization). Here, both the AS and SLF models show fairly good agreement with MLAYER. For vertical polarization, the MT model slightly overestimates the losses by approximately 8 dB at some heights.

# 5.0 DISCUSSION

In this section, some of the advantanges and disadvantages of the rough surface models presented in Section 2.0 will be discussed, along with possible reasons why some of the discrepancies, shown in the previous section, occurred between these models and MLAYER.

## 5.1 MIXED TRANSFORM ALGORITHM

One of the disadvantages of the MT model is that it is dependent on the incident angle at the boundary. This is a ray theory approach in which it is assumed there is a dominant mode, and hence, a single grazing angle, being propagated within the duct. The grazing angle is not explicitly available within the split-step algorithm; therefore, spectral estimation procedures must be used to determine this parameter. Whether a sophisticated algorithm, such as MUSIC is used, or a simple FFT procedure, as used here, this additional calculation must be performed nevertheless.

For many surface or surface-based ducts, the assumption of a dominant mode being propagated may be a reasonable one. As shown in figure 1, the grazing angles calculated vs. range for the 45.7-meter surface duct are fairly constant beyond 10 km. As determined from MLAYER, there are 15 eigenangles corresponding to the multiple modes propagated within the duct, with 10 of these modes being equally dominant. For this environment, the assumption of a single mode is sufficient to yield reasonable results. However, this is not the case for the evaporation duct. There are 27 modes calculated by MLAYER (for the case corresponding to figures 18a and 18b) being propagated within the duct, over half of which are fairly dominant, with varying attenuation rates. Obviously, a single-mode theory is not sufficient for this refractivity environment. This may be one reason there was poor agreement between the MT model and MLAYER for this case.

Another problem with the MT model is in the numerical implementation of the algorithm itself. Dockery (*op. cit.*) states that a singularity may occur in the fractional term $\left(\alpha^2 + p^2\right)^{-1}$ for large waveheights and close ranges. This is due to the rough surface factor, $\rho_o$, which causes the reflection coefficient to become very small, resulting in $\alpha$ becoming purely imaginary. Spikes occur in the calculated values of these fractional terms, and if severe enough, will not be properly transformed by the FFTs. A "quick fix" has been implemented in TEMPER to keep the real part of $\alpha$ from becoming too small. Specifically, $|\alpha_r|$ is restricted to values larger than 1/20 of the smooth sea value. This 1/20 cut-off value was arbitrarily chosen, but as the author states, "it has been found to eliminate severe spikes in the calculation of the troublesome factors while still allowing rough surface effects to be represented accurately."

While this may be true for most cases, this factor did not seem to be the optimum one for some of the cases presented in Section 4.0. Consider the case shown in figure 19b. For a high wind speed of 20 m/s (2.0-meter waveheight) the MT result underestimated the loss compared with MLAYER. Whereas, for the 10-m/s case (figure 16b), there was good agreement. The reason for the discrepancy shown in figure 19b is likely due to the numerical problems just mentioned, i.e., the 1/20 factor may be too large a cut-off in this case. As an experiment, a cut-off value of 1/30 was used instead; the result is shown in figure 27. This improved the comparison with MLAYER substantially. This is not to say that a 1/30 cut-off should be used for all cases. For the large discrepancy shown in figure 25b, this same 1/30 cut-off improved the MT result just slightly. By trial-and-error, a cut-off value of 1/200 was found that resulted in very good

agreement with MLAYER for receiver heights greater than 40 meters. The MT results using both these cut-off values, along with MLAYER, are shown in figure 28. Restricting $|\alpha_r|$ to 1/200 the smooth sea value is still two orders of magnitude greater than that calculated by Eq. 2; therefore, there is a lot of flexibility in the cut-off values that can be chosen for these cases. Again, this is another disadvantage in using this method; a chosen cut-off value may seem to work for most cases, but there may always be some environment or frequency/wind-speed combination for which this value may not be optimum.

Lastly, the MT model is a very time-consuming algorithm. Both the cosine and sine transforms are needed to determine the field at each range step. While this is unavoidable if finite conductivity and rough surface effects are to be accurately modeled, it nevertheless makes for a very impractical operational model. It is somewhat faster to model finite conductivity only, since the term is independent of grazing angle (using a small-angle approximation) and the additional calculations to determine grazing angle need not be performed.

The greatest advantage of this model is that it is the most accurate split-step PE model for finite conductivity and rough surface effects known to the authors of this report. It is an excellent tool as a research/laboratory model and is much more efficient than such waveguide models as MLAYER. However, problems with the restrictions on $|\alpha_r|$ mentioned above should be investigated further.

## 5.2 SURFACE LOSS FUNCTION

While the SLF model does not depend on a *single* grazing angle (and hence the assumption of a dominant mode), it does assume that the spectral decomposition of the field is appropriately attenuated by the loss function as determined by the $p$-space angles within the surface layer. No concrete explanation can be given as to why this model did not work as well for the evaporation duct environment as it did for the surface duct environment. However, one possibility may be that when dealing with a more complicated refractivity environment, which results in a good number of modes being propagated, the SLF model cannot sufficiently account for the attenuation of all the modes. This is seen from the fact that there were almost twice as many modes being propagated for the evaporation duct as for the surface duct (as determined by MLAYER).

Another disadvantage of this model is in determining the optimum height, $d$, for the surface layer. Moore-Head, Jobst, and Holmes [9] suggest estimating $d$ from the Rayleigh resolution criterion for linear diffractors, $\frac{\lambda}{d} = \phi$, where $\lambda$ is the wavelength in meters and $\phi$ is the angle to be resolved. For the cases presented in Section 4.0, a maximum propagation angle of 1.3 degrees was used, making the mesh height, $\Delta z$, 0.64 meter at 10 GHz and 0.32 meter at 20 GHz. The surface and transition layers ($2d$) were chosen to correspond to $16\,\Delta z$, making $d$=5.2 meters at 10 GHz, $d$=2.6 meters at 20 GHz, and $\phi$=0.33 degrees. For the most part, these values for $d$ seemed to work well; large differences, however, can occur in the results if too small or too large a value for $d$ is chosen. Figure 29 shows a comparison with MLAYER corresponding to figure 20a, with additional SLF results using 8-pt ($d$=2.6 meters) and 32-pt ($d$=10.3 meters) surface layers. The differences are substantial.

An advantage to using this model is that it is simple to implement and can also adequately model vertical polarization and finite conductivity. As an example, the loss function, $L(p)$, was slightly modified to include the magnitude of the Fresnel (vertical polarization) reflection coefficient: $L(p) = (|R_v|^{\frac{1}{N}})^N$. Figure 30 compares the SLF model with MLAYER for the surface duct

environment using vertical polarization and a smooth surface. A long receiver range of 400 km is used for this case to show the large difference occuring between horizontal and vertical polarization for MLAYER. The SLF model shows excellent agreement for this case.

Along with ease of implementation, this is a more efficient model than the MT model since only sine transforms are needed to determine the solution. The field is initially determined by using a smooth, perfectly conducting boundary, which produces a solution with odd symmetry. Therefore, the field is propagated by using only sine transforms, and all finite conductivity and rough surface effects are accounted for by applying the loss function, $L(p)$.

## 5.3 APPROXIMATE SOLUTION

Mathematically, the AS model may be the best one to use, since it is grazing angle-independent; its main disadvantage, however, is that it is the poorest performer of the three. This is not due to the mathematical derivation of the algorithm, but perhaps to the numerical implementation. For instance, the surface mixing length, $L_s$, given by Eq. 9, may not be the best choice. To demonstrate, the same test case will be used as shown in figure 30, in which vertical polarization and smooth surface are assumed. Although only horizontal polarization and perfect conductivity have been presented for this model, the AS model is well-suited for modeling finite conductivity and vertical polarization. From Eqs. 1, 5, and 7, the impedance boundary condition for a finite-conducting, rough surface is simply

$$\psi(z = 0, r) + \left[\eta(r) - \frac{in_c}{k_o}\right]\frac{\partial\psi(r,z)}{\partial z}\bigg|_{z=0} = 0$$

In which case, Eq. 8 is replaced with

$$10^{-6}M(z) - \left[\eta(r) - \frac{in_c}{k_o}\right]\frac{\delta''(z)}{2k_o^2}$$

A smooth surface will be used for this case so that no question will arise about the validity of the sea wave spectrum and the realization of $\eta(r)$ being implemented in the model. The only parameter now in question is $\delta''(z)$—specifically, the surface mixing length, $L_s$, used in its implementation.

Figure 31 shows the AS model vs. MLAYER for vertical polarization. The MLAYER result for horizontal polarization is also shown. Here, the AS model agrees poorly with MLAYER and shows just slightly more attenuation than the horizontal polarization result. $L_s$ is continually varying, since it is determined by the field at each range step. The amount of variation is shown in figure 32, which displays $L_s$ vs. range. A second comparison was made for the same case as in figure 31; however, $L_s$ was arbitrarily chosen to be constant and equal to the mesh height—in this case, 0.64 meter. The result is shown in figure 33. There is much better agreement with the vertical polarization result for MLAYER, but much more oscillation appears in the field at higher heights. Further investigation should be made to determine the best choice for $L_s$. This parameter may be just one among others (in the numerical implementation of the rough surface model) to contribute to the poor agreement with MLAYER for the cases presented in Section 4.0.

The biggest attraction in using this model is that it is the most numerically efficient of the three. All environmental effects (i.e., refractivity, finite conductivity, rough surface) are included in a single exponential term, which need only be computed once (for a range-independent case) in the initial calculation of the field. Also, the field is propagated by using only sine transforms.

# 6.0 CONCLUSIONS AND RECOMMENDATIONS

The split-step PE rough surface models investigated in this paper were compared with a waveguide model, MLAYER, for two homogeneous refractivity environments and wind speeds of 10 m/s and 20 m/s. MLAYER was shown to accurately predict radiowave fields in the presence of strong wind speeds and was, therefore, used as a reference model. The MT and SLF models consistently agreed with results given by MLAYER; however, the AS model showed the poorest agreement, giving differences in predicted field values as much as 40 dB for some cases. While all three methods can model finite conductivity and vertical polarization, only the MT model has shown it can accurately do this.

The MT model is dependent on the incident angle of the field at the boundary. Since the grazing angle cannot be explicitly determined within the split-step algorithm, some form of spectral estimation must be performed. The single-mode assumption that this implies can lead to incorrect results for some cases, as discussed in Section 5.1. The SLF and AS models are more advantageous to use in this respect, since they are not dependent on a single grazing angle. The AS model relies on a statistical knowledge of the sea surface to determine the field, and the SLF model uses a mode theory approach in attenuating the field below a surface layer. However, further investigation needs to be done in order to determine the optimum height of this layer for varying frequencies and refractivity environments.

The MT model is, perhaps, the most mathematically rigorous of the three, yet it is the least efficient whereas the AS model is the most numerically efficient but shows the poorest match to MLAYER. In using one of these methods to model rough surface effects, whether it be over ocean or variable terrain, a satisfactory compromise may be to use some form of the SLF model, since it is shown to agree fairly well with MLAYER and is still numerically efficient.

A split-step PE model that uses the MT model would be an excellent research/laboratory tool, since it is still more numerically efficient than current waveguide models and has been shown to consistently match waveguide results. As an operational model, some form of the SLF model would most likely be the best choice.

# 7.0 REFERENCES


1. Kuttler, J.R., and G.D. Dockery, "Theoretical description of the parabolic approximation/ Fourier split-step method of representing electromagnetic propagation in the troposphere," *Radio Sci.*, pp. 381-393, March–April, 1991.

2. Levy, M.F., "Parabolic equation modelling of propagation over irregular terrain," *Seventh Int'l Conf. on Ant. and Prop.* (ICAP 91), U.K., 15–18 April 1991.

3. Barrios, A.E., "A Terrain Parabolic Equation Model for Propagation in the Troposphere," accepted for publication in *IEEE Ant. and Prop.*

4. Tappert, F.D., "The parabolic approximation method," in *Wave Propagation and Underwater Acoustics* (Lecture Notes in Physics), J.B. Keller and J.S. Papadakis, Eds. New York: Springer-Verlag, vol. 70, pp. 224–287, 1977.

5. Baumgartner, G.B., "XWVG: A Waveguide Program for Trilinear Tropospheric Ducts," San Diego, CA, NOSC TD 610, June 1983.

6. Miller, A.R., R.M. Brown, and E. Vegh, "New derivation for the rough-surface reflection coefficient and for the distribution of sea-wave elevations," *IEE Proc.*, vol. 131, No. 2, pp. 114–116, April 1984.

7. Phillips, O.M., *Dynamics of the Upper Ocean*, Cambridge University Press, London, 1966.

8. Report 1008-1, "Reflection from the surface of the Earth," Volume V of Recommendations and Reports of the CCIR, XVIIth Plenary Assembly, ITU, Geneva, 1990.

9. Moore-Head, M.E., W. Jobst, and S. Holmes, "Parabolic equation modeling with angle-dependent surface loss," *JASA*, vol. 8, No. 1, pp. 247–251, July 1989.

10. Richter, J.H., and H.V. Hitney, "Antenna Heights for the Optimum Utilization of the Oceanic Evaporation Duct; Part III: Results from the Mediterranean Measurements," San Diego, CA, NOSC TD 1209, vol. 2, January 1988.

11. Paulus, R.A., "Specification for Environmental Measurements to Assess Radar Sensors," San Diego, CA, NOSC TD 1685, November 1989.

12. Rino, C.L., T.L. Crystal, A.K. Koide, H.D. Ngo, H.D., and H. Guthart, "Numerical simulation of backscatter from linear and nonlinear ocean surface realizations," *Radio Sci.* 26, pp. 51–71, 1991.

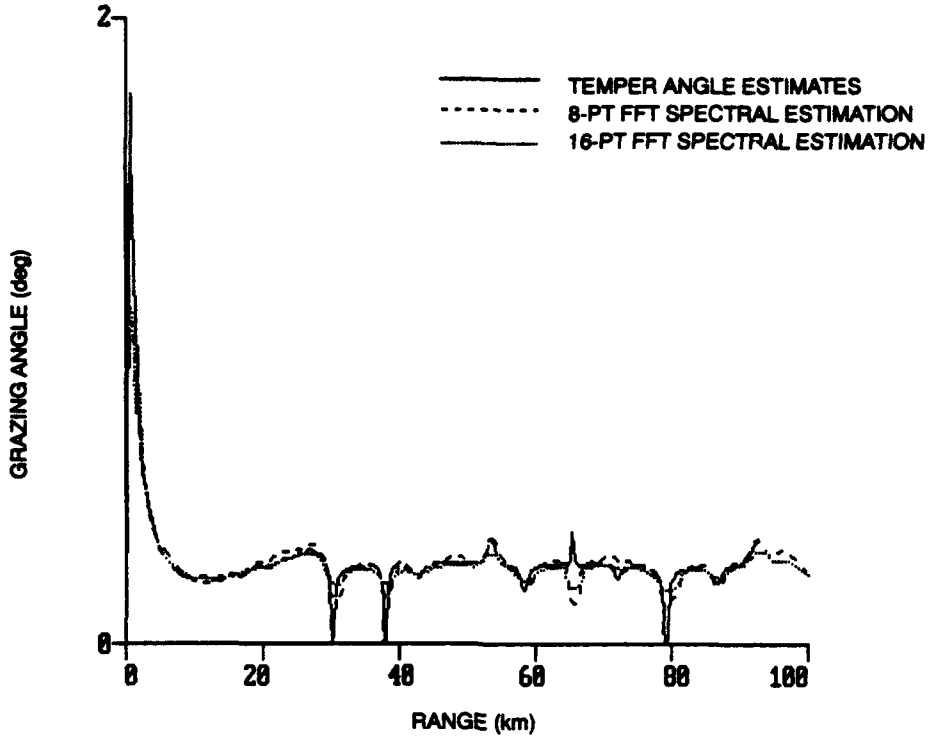


Figure 1. Grazing angle vs. range for 45.7-meter surface duct, 10 GHz. Antenna height at 22.9 meters.

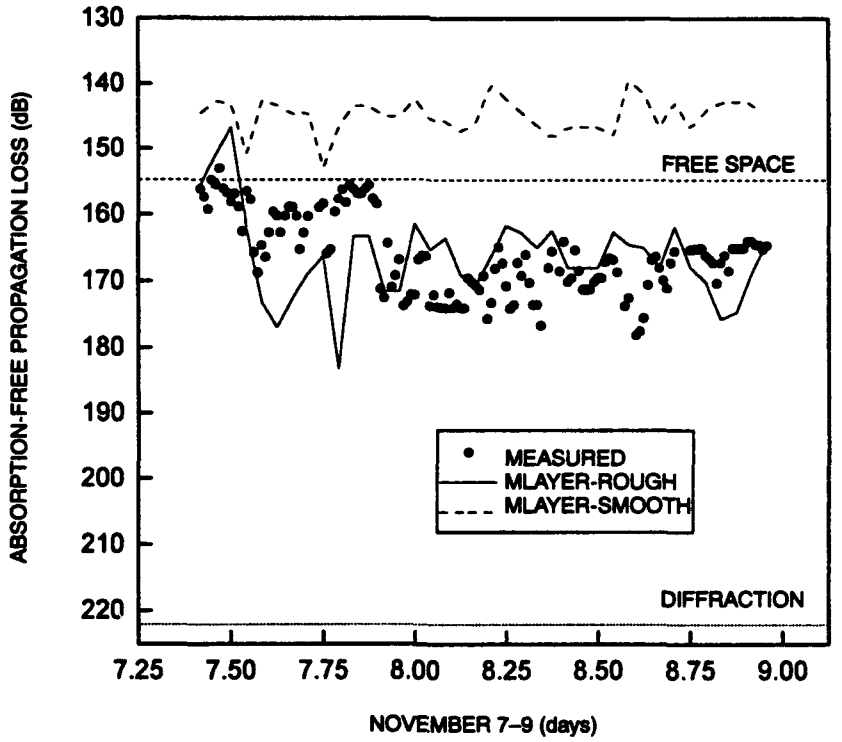


Figure 2. Predicted and measured absorption-free loss vs. time for November 7–9, 1972, 37.44 GHz, receiver height at 3.6 meters.

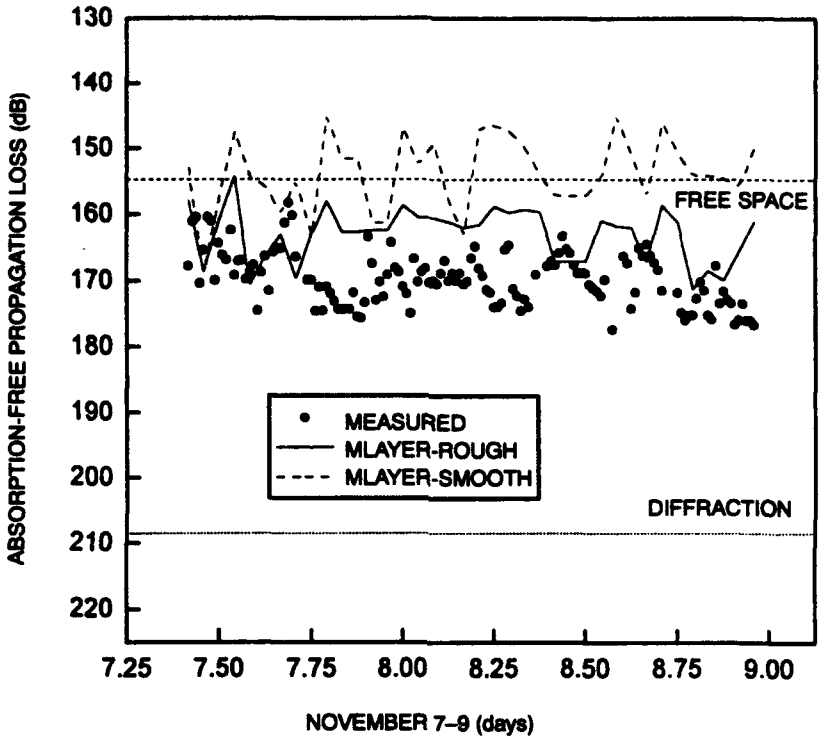


Figure 3. Prediction and measured absorption-free loss vs. time for November 7–9, 1972, 37.44 GHz, receiver height at 8.6 meters.

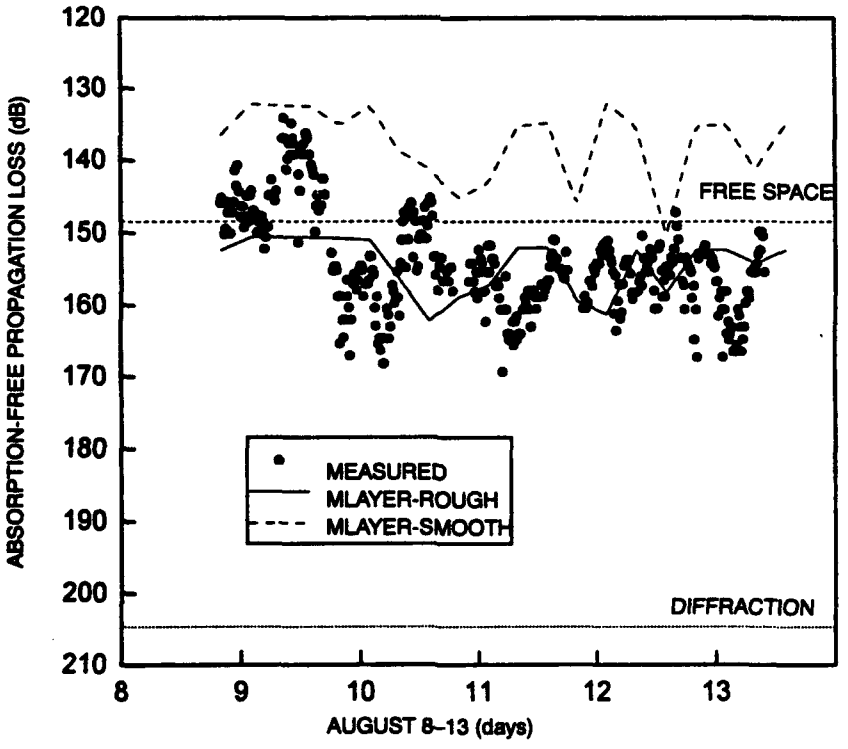


Figure 4. Predicted and measured absorption-free loss vs. time for August 8–13, 1972, 17.96 GHz, receiver height at 4.3 meters.

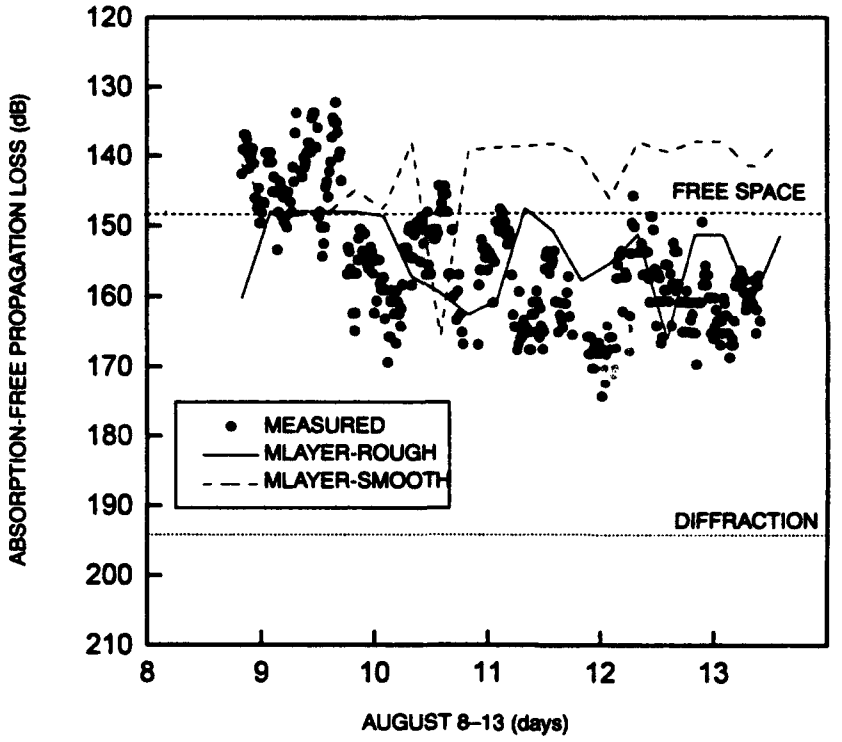


Figure 5. Predicted and measured absorption-free loss vs. time for August 8–13, 1972, 17.96 GHz, receiver height at 9.5 meters.

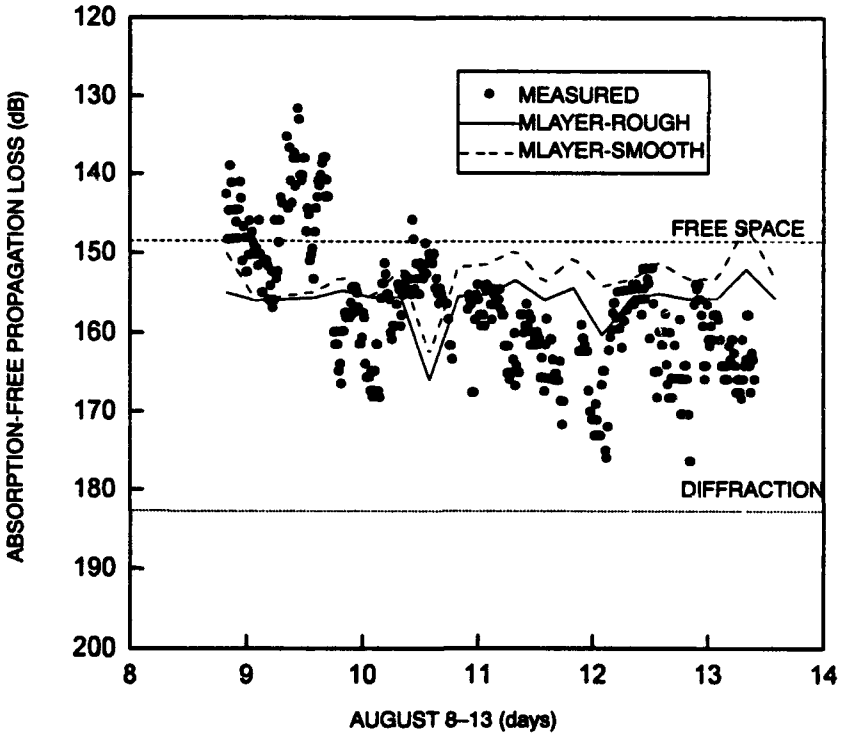


Figure 6. Predicted and measured absorption-free loss vs. time for August 8–13, 1972, 17.96 GHz, receiver height at 17.8 meters.

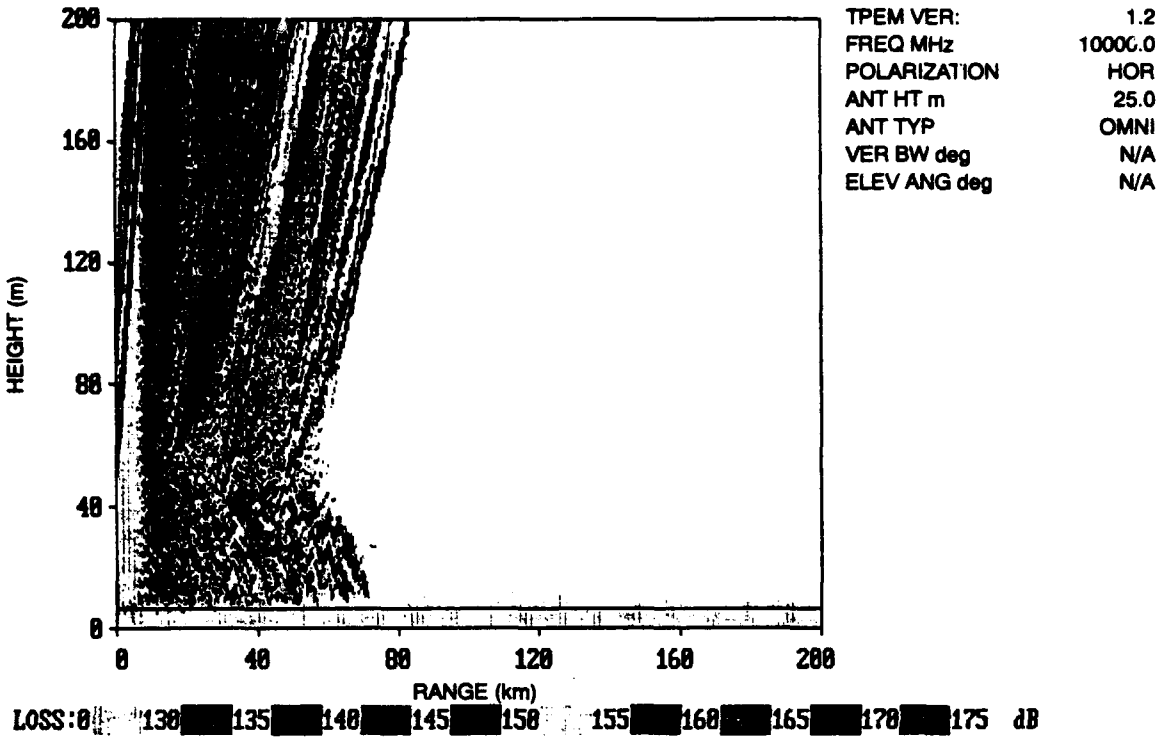


Figure 7. Coverage diagram from TPEM for sea surface realization at 20-m/s wind speed, 45.7-meter surface duct, 10 GHz.

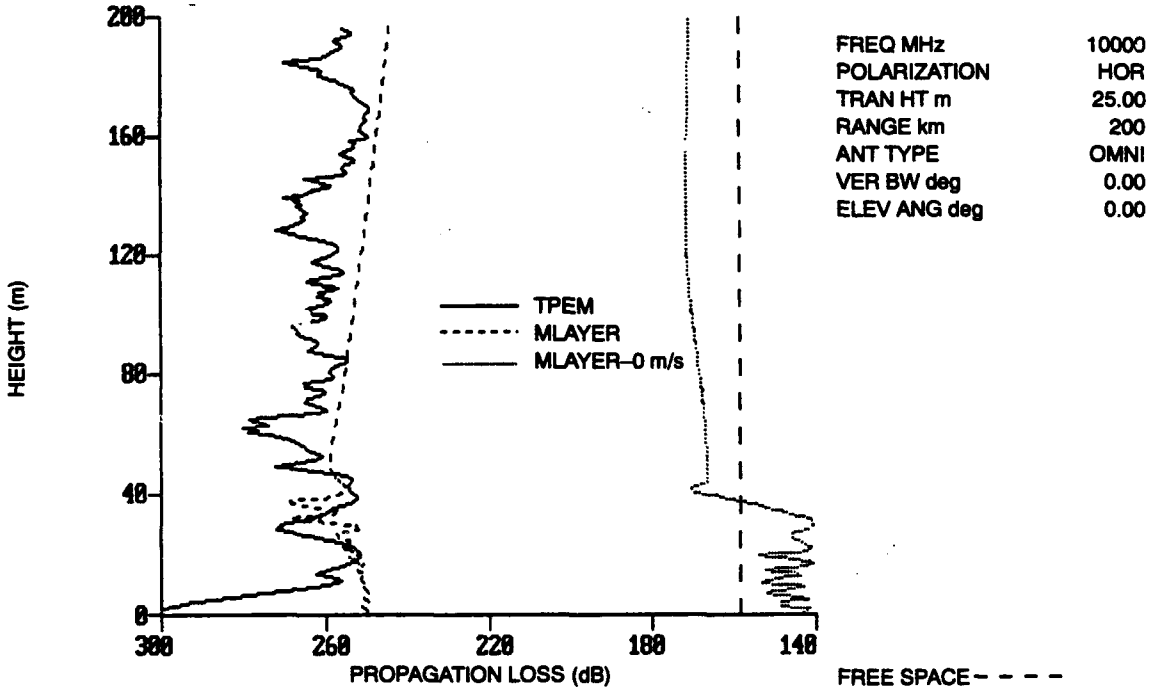


Figure 8. Height vs. propagation loss comparing TPEM with MLAYER at receiver range of 200 km for case shown in figure 7.

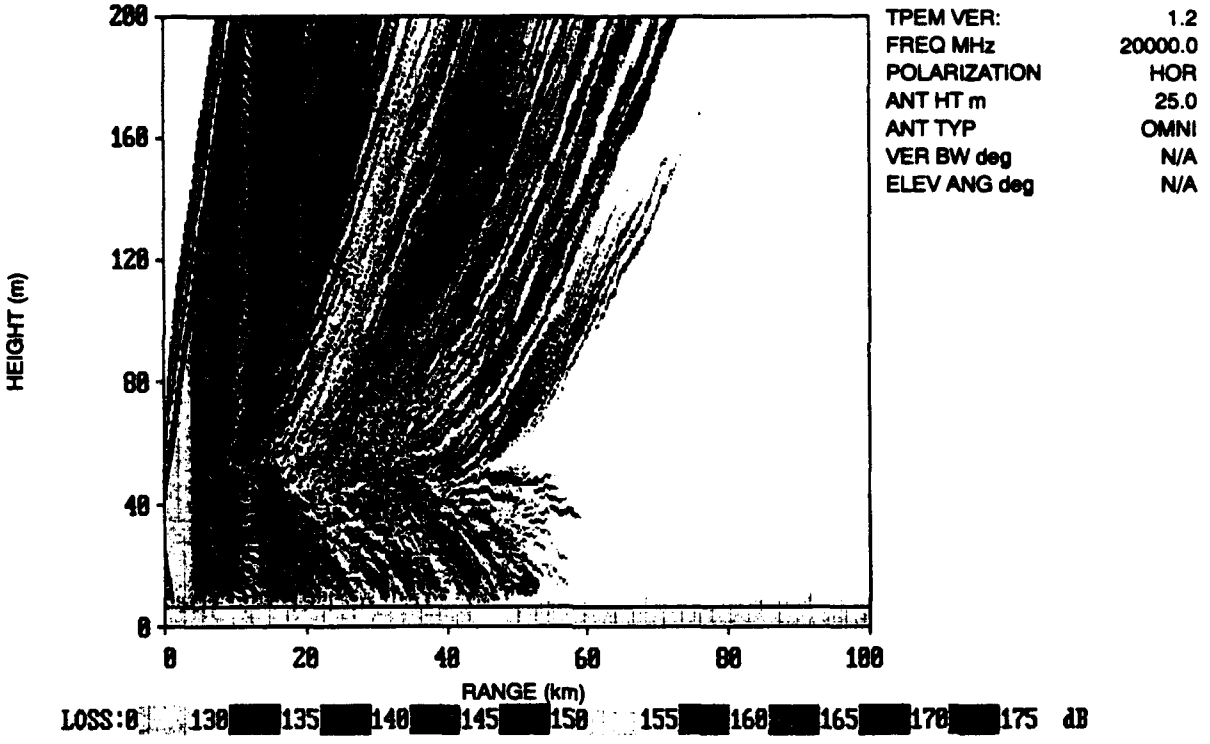


Figure 9. Coverage diagram from TPEM for sea surface realization at 20-m/s wind speed, 45.7-meter surface duct, 20 GHz.

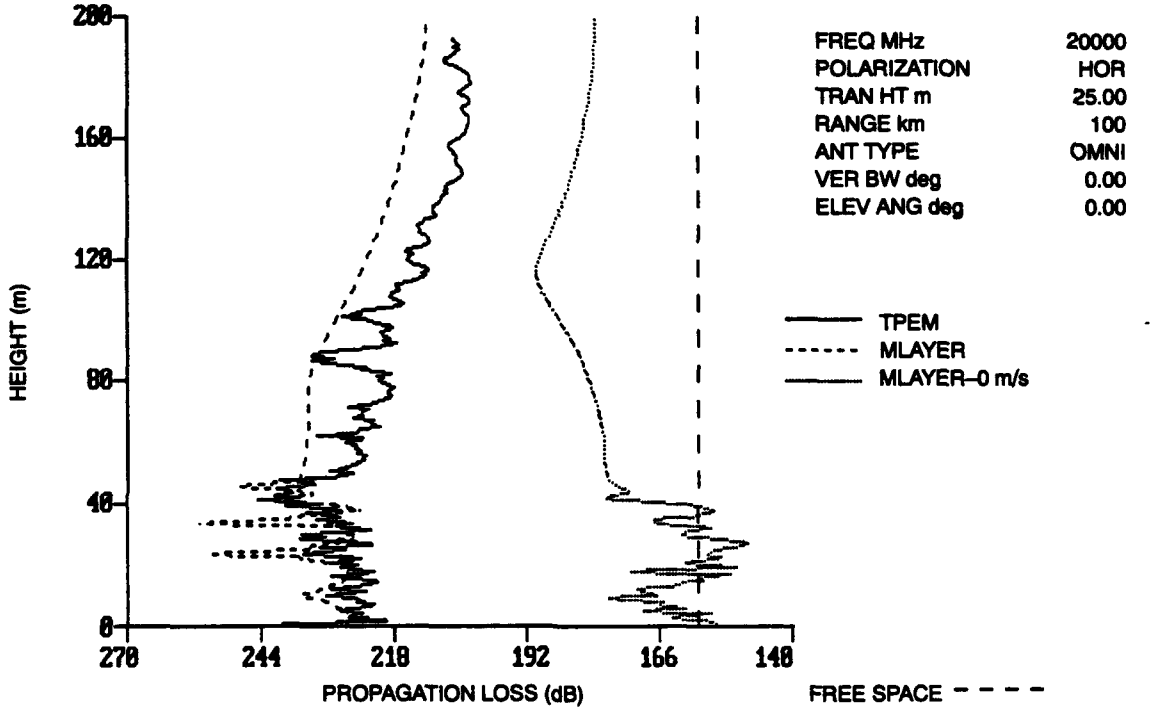


Figure 10. Height vs. propagation loss comparing TPEM with MLAYER at receiver range of 100 km for case shown in figure 9.

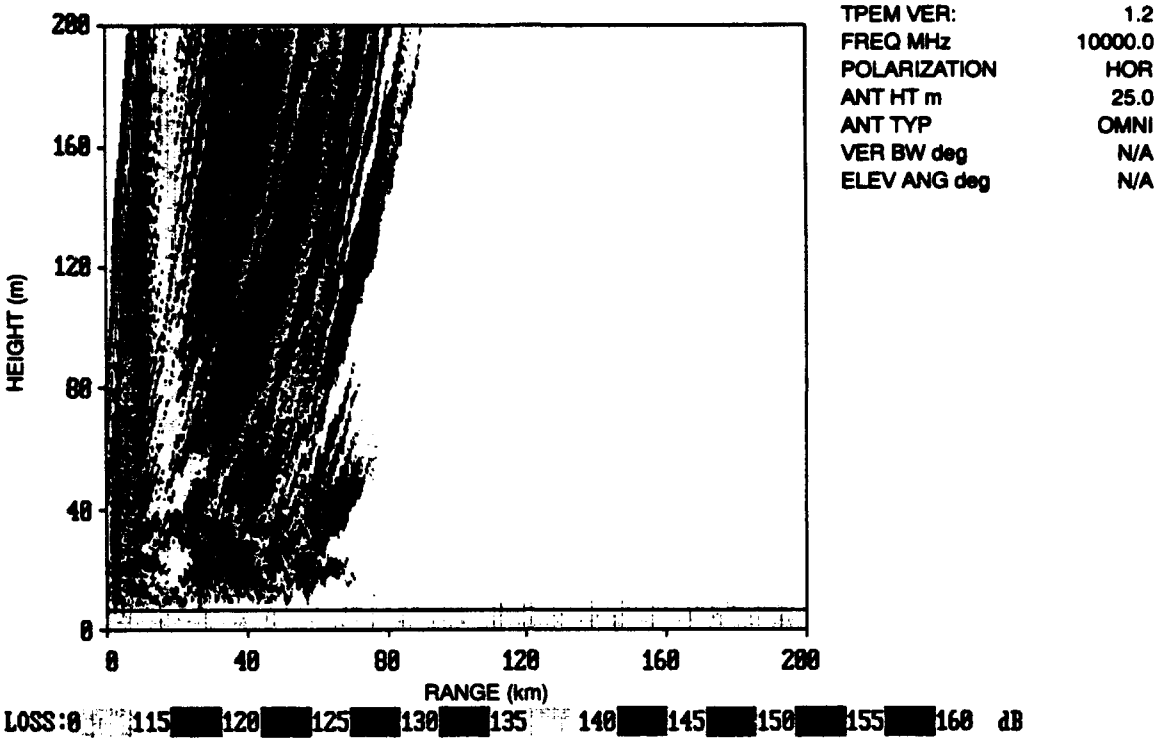


Figure 11. Coverage diagram from TPEM for sea surface realization at 20-m/s wind speed, 24-meter evaporation duct, 10 GHz.

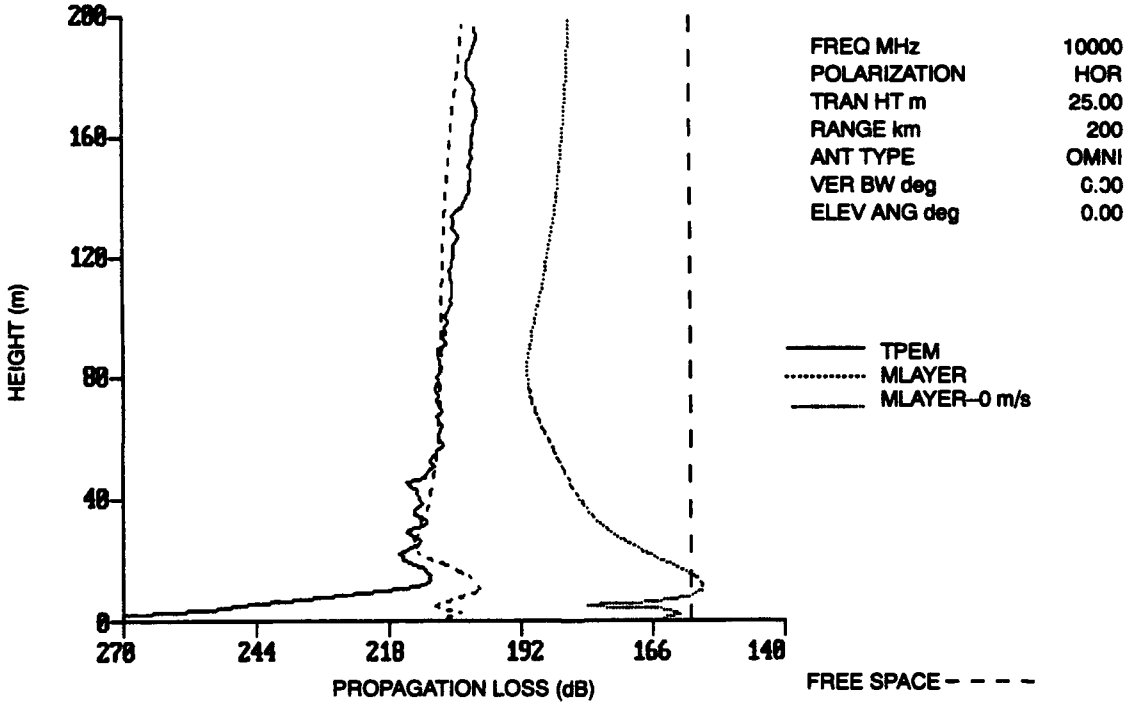


Figure 12. Height vs. propagation loss comparing TPEM with MLAYER at receiver range of 200 km for case shown in figure 11.

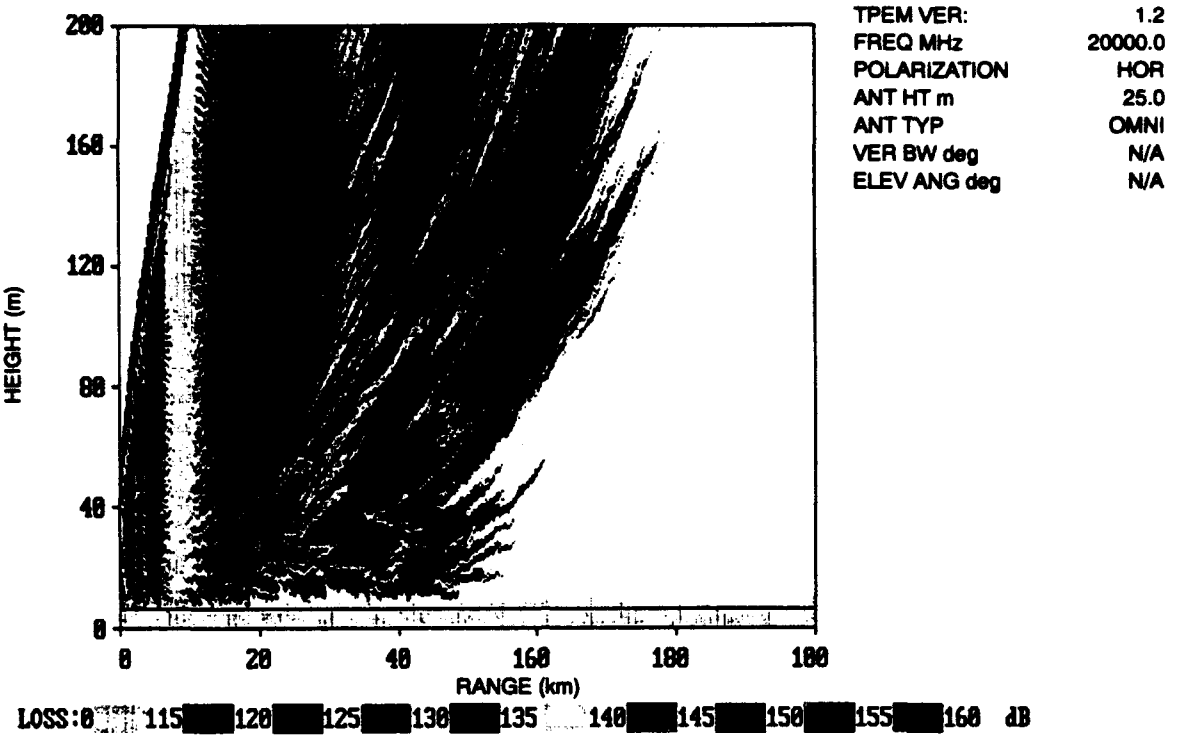


Figure 13. Coverage diagram from TPEM for sea surface realization at 20-m/s wind speed, 24-meter evaporation duct, 20 GHz.

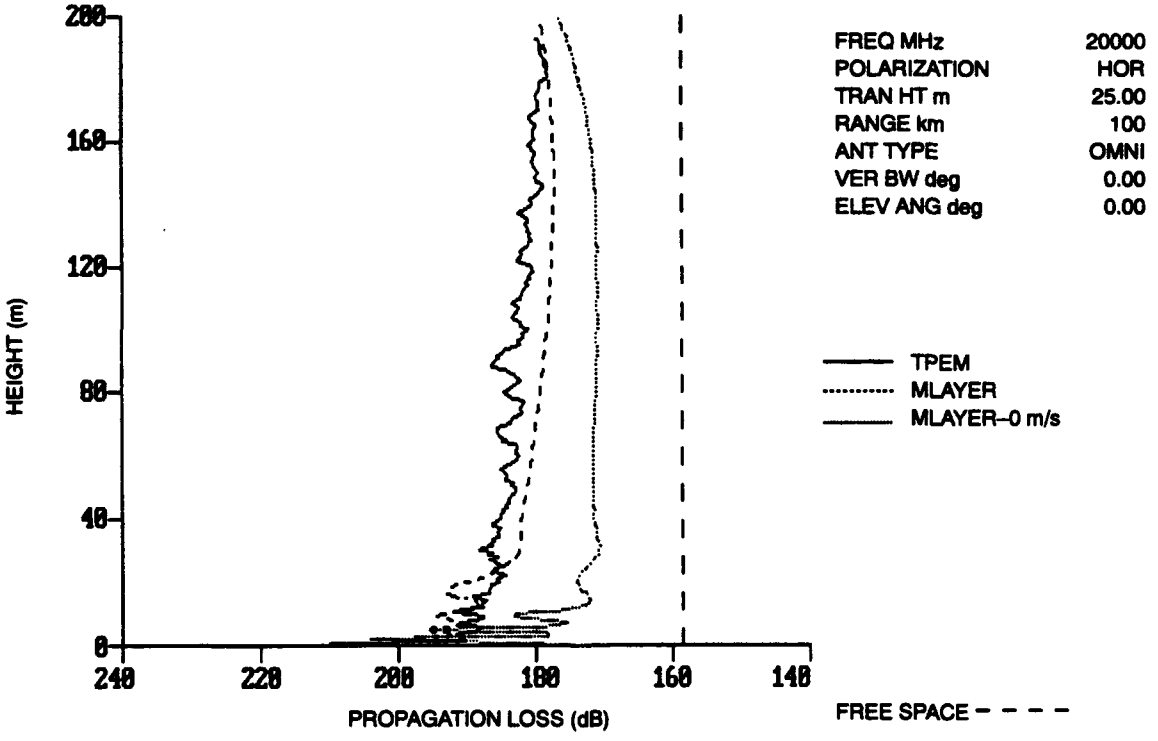


Figure 14. Height vs. propagation loss comparing TPEM with MLAYER at receiver range of 100 km for case shown in figure 13.

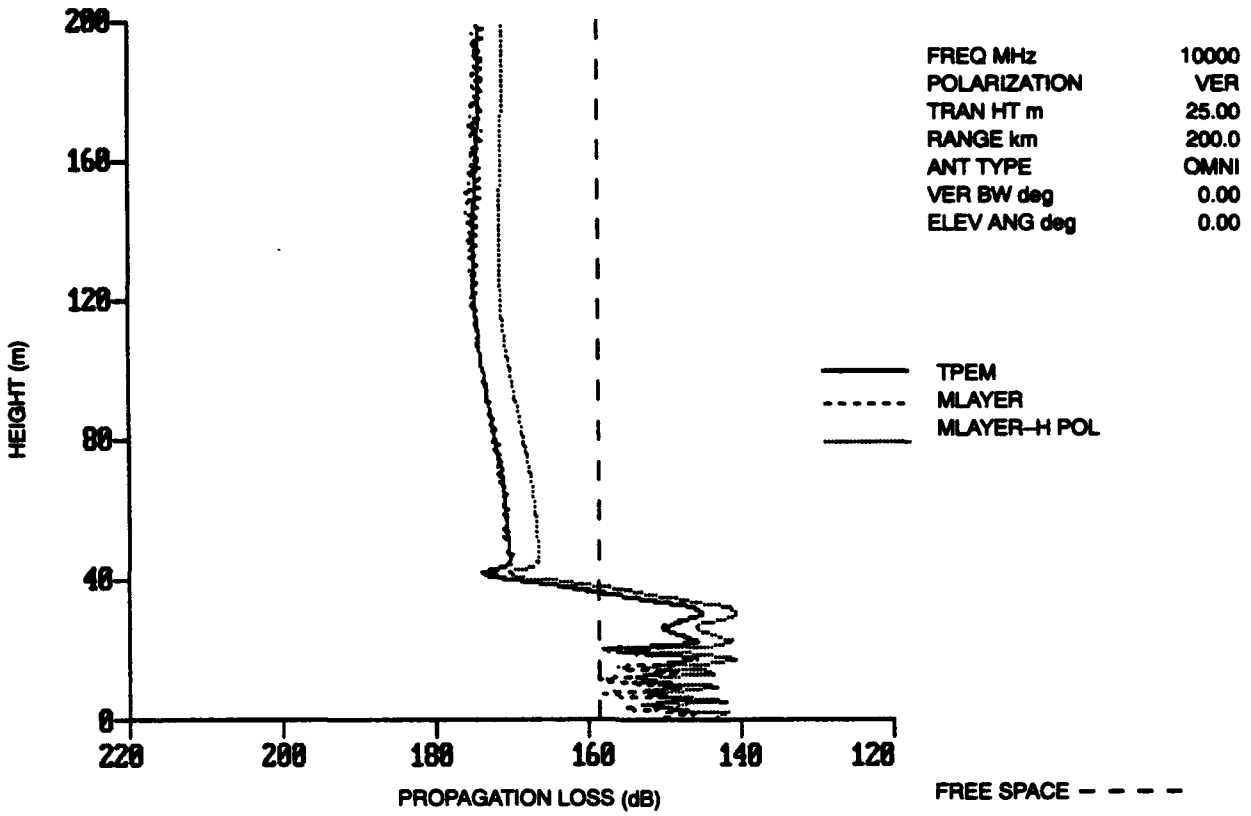


Figure 15. MT vs. MLAYER for smooth surface and vertical polarization, 45.7-meter surface duct, 10 GHz.

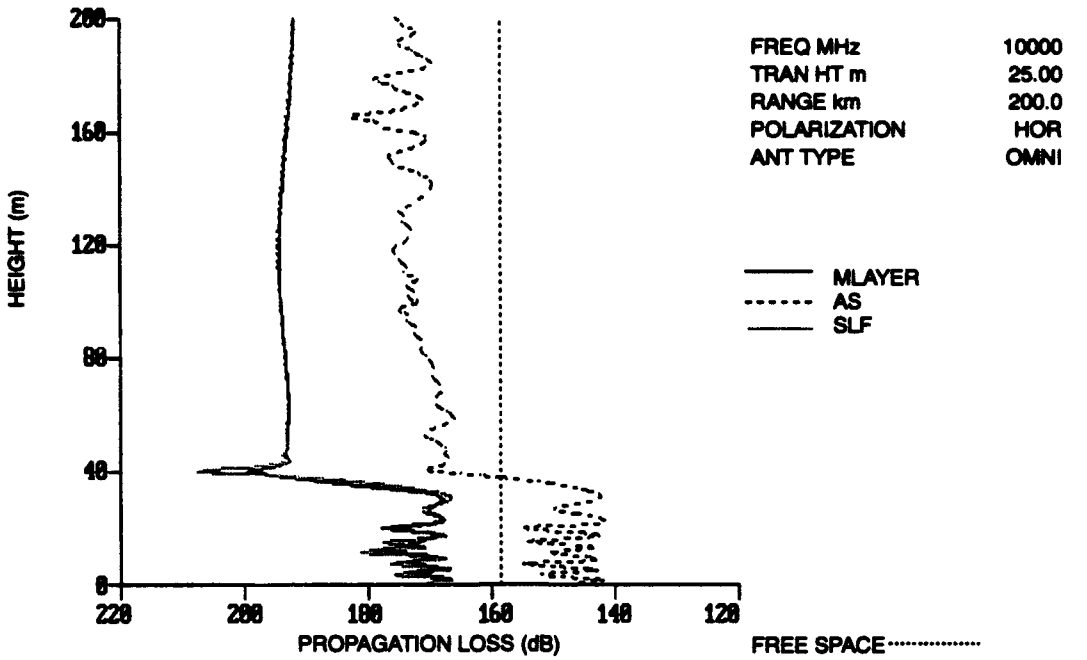


(a)

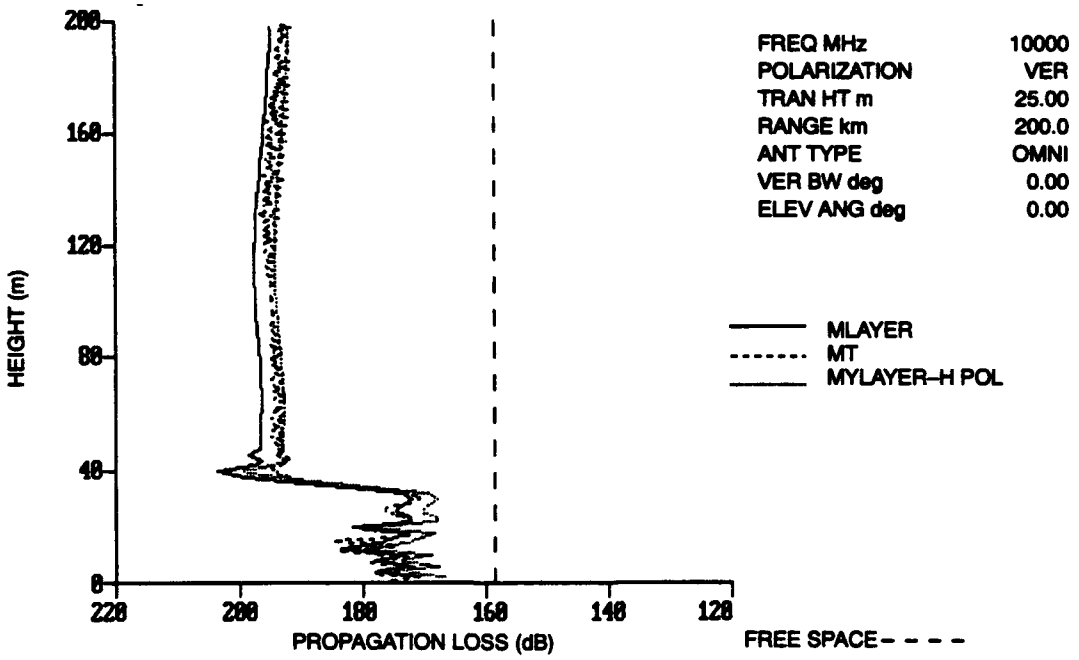


(b)

Figure 16. MLAYER results for 10 GHz, 10-m/s wind speed, 45.7-meter surface duct vs. (a) AS and SLF and (b) MT.

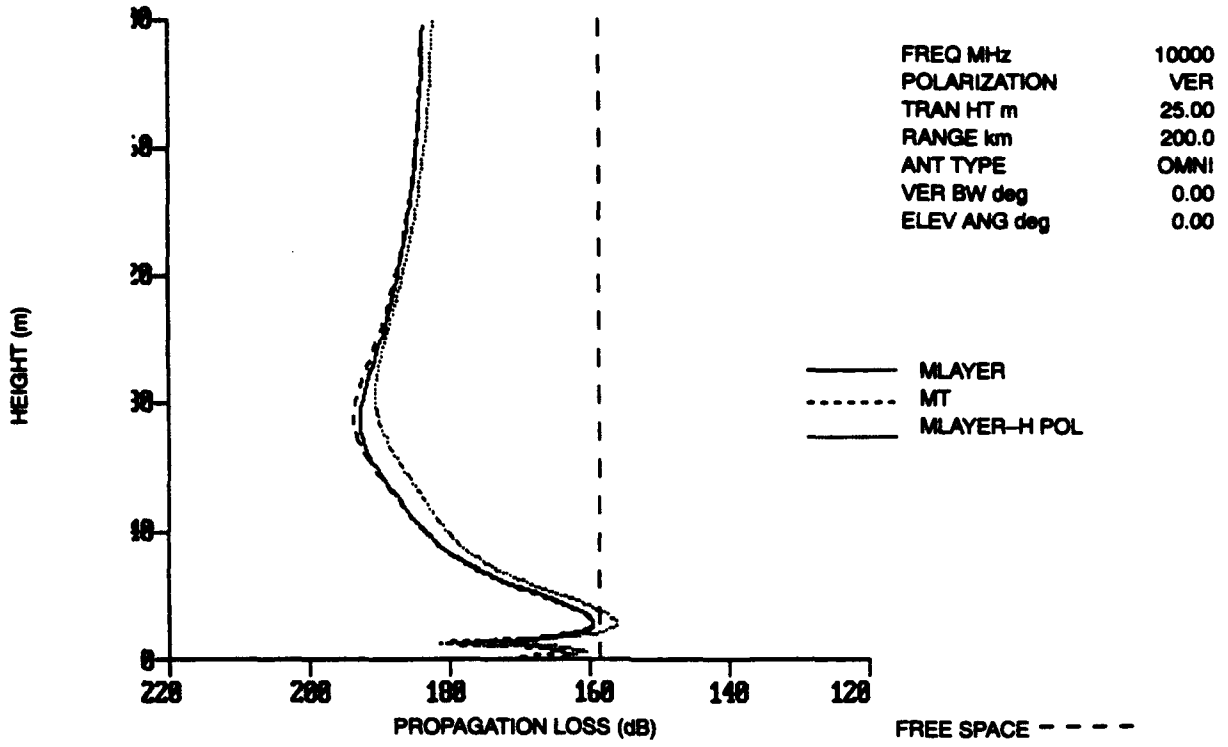


Figure 17. MT vs. MLAYER for smooth surface and vertical polarization, 24-meter surface duct, 10 GHz.

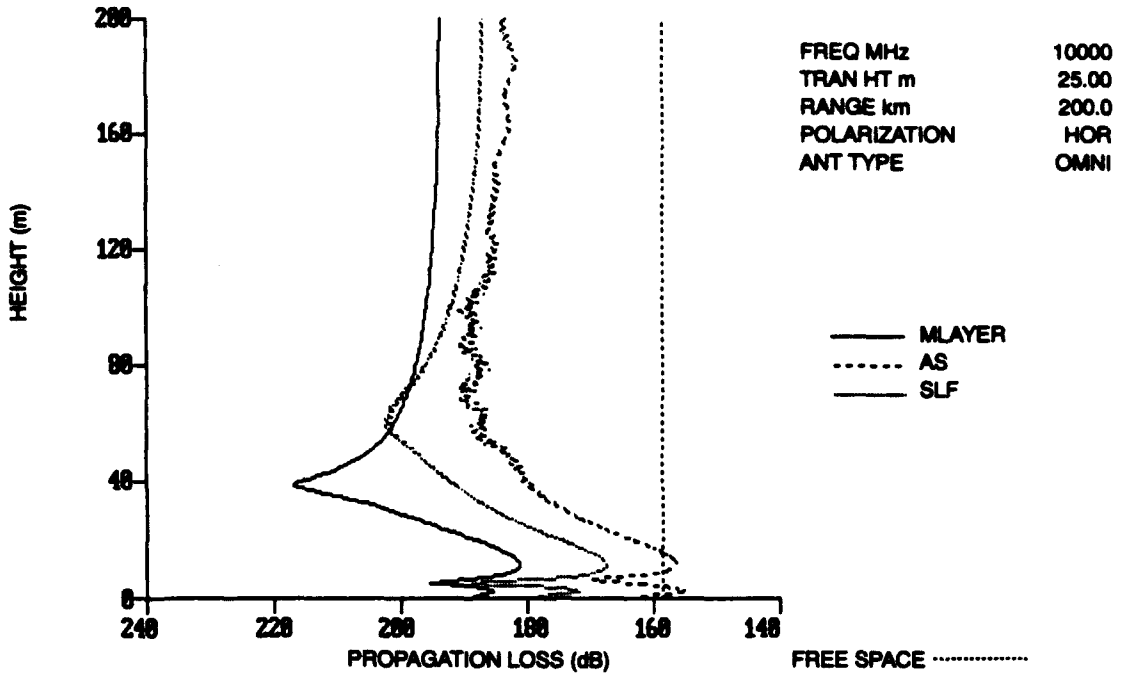


(a)

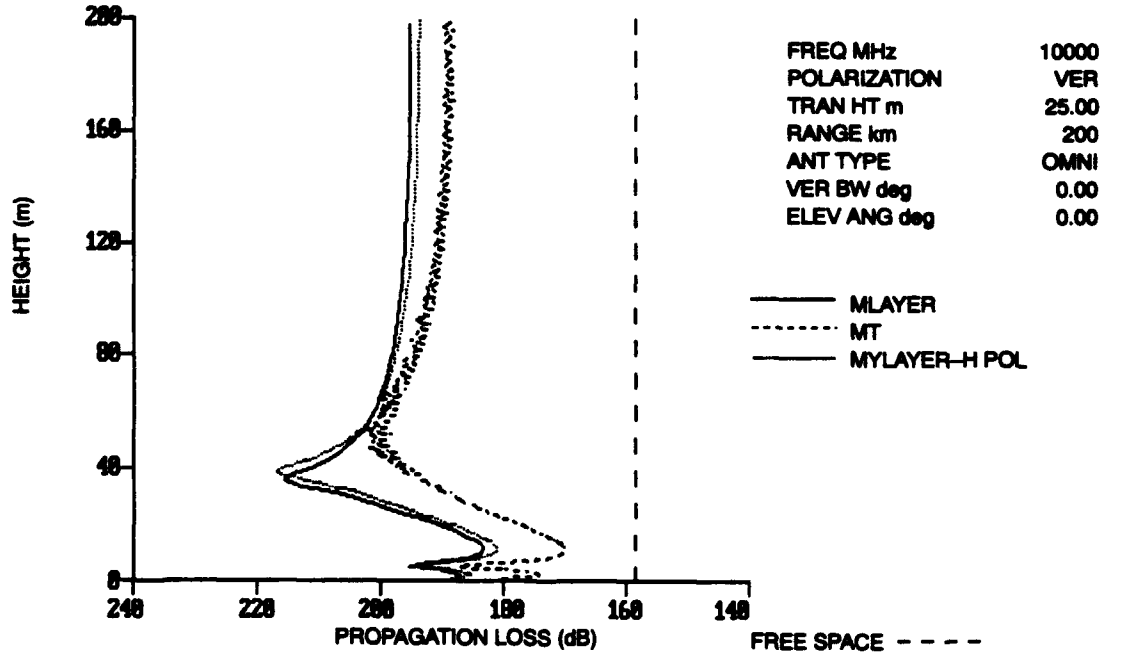


(b)

Figure 18. MLAYER results for 10 GHz, 10-m/s wind speed, 24-meter evaporation duct vs. (a) AS and SLF and (b) MT.

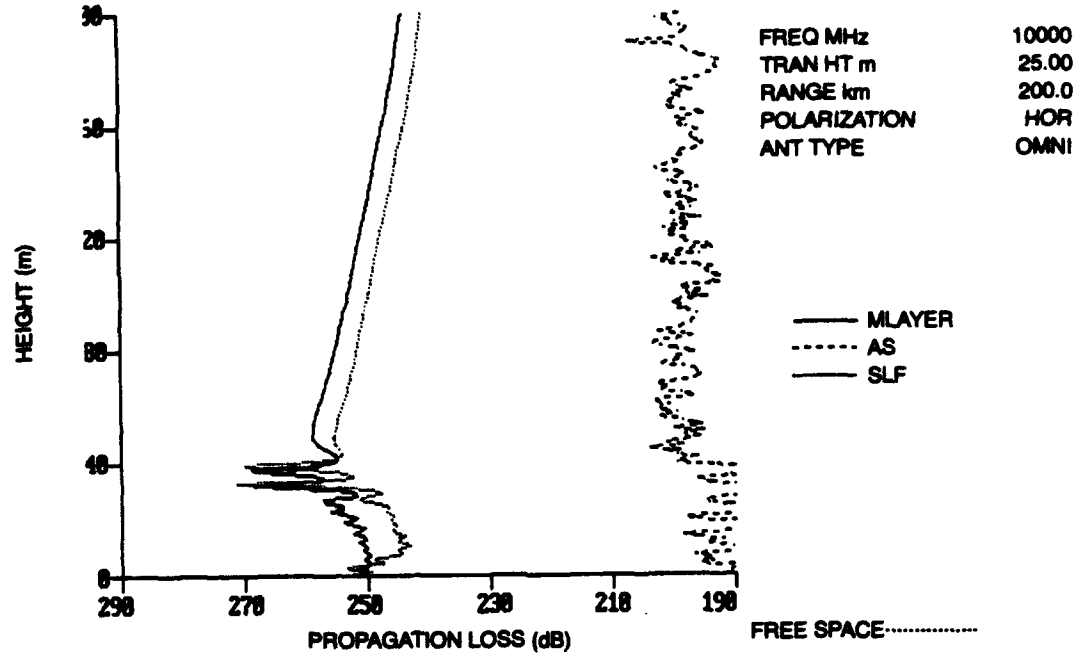


(a)

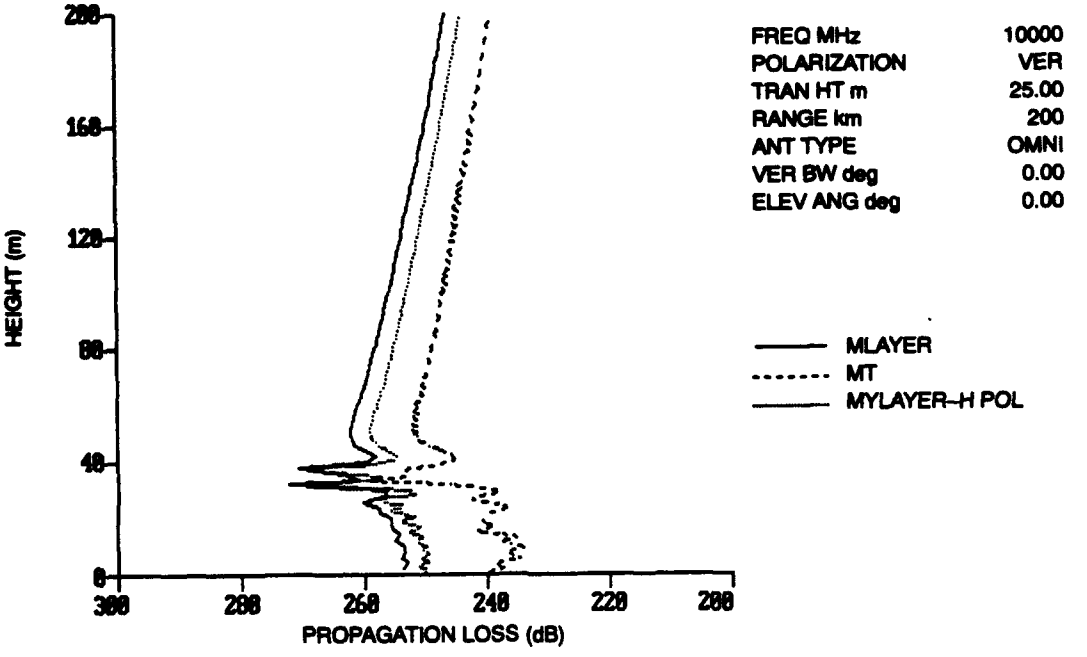


(b)

Figure 19. MLAYER results for 10 GHz, 20-m/s wind speed, 45.7-meter surface duct vs. (a) AS and SLF and (b) MT.

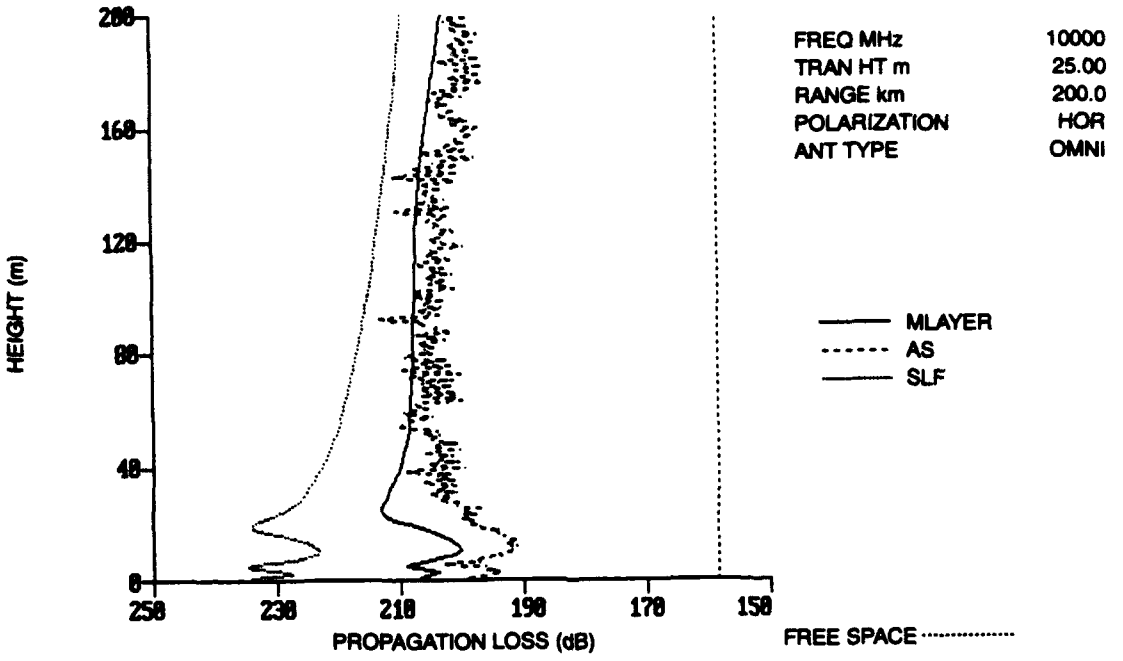


(a)

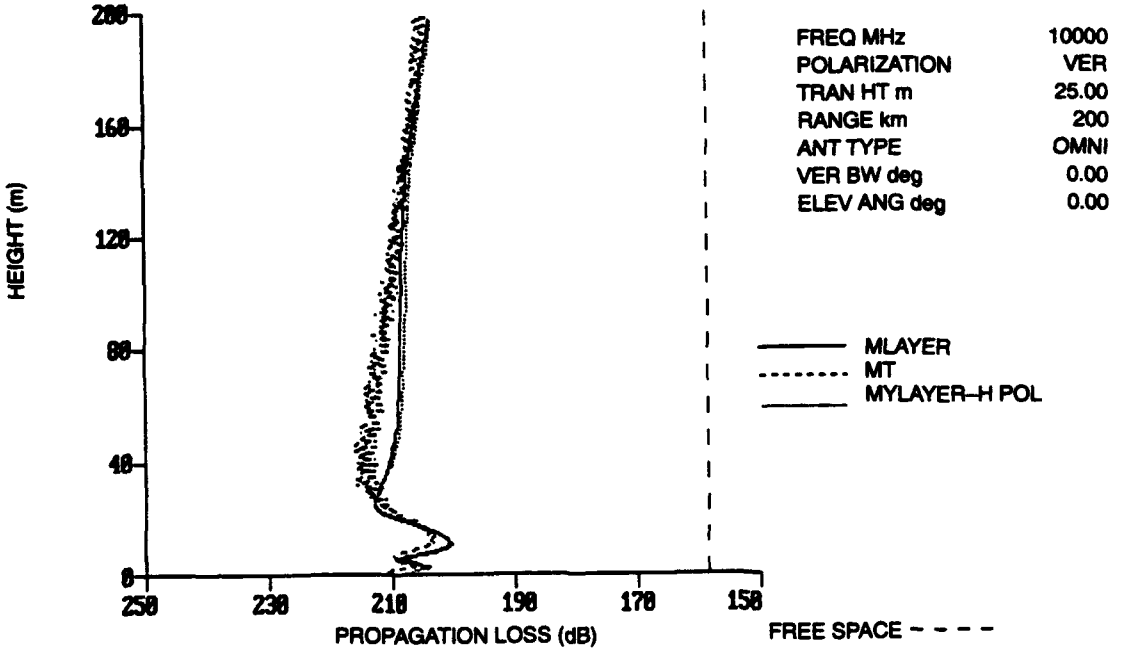


(b)

Figure 20. MLAYER results for 10 GHz, 20-m/s wind speed, 24-meter evaporation duct vs. (a) AS and SLF and (b) MT.

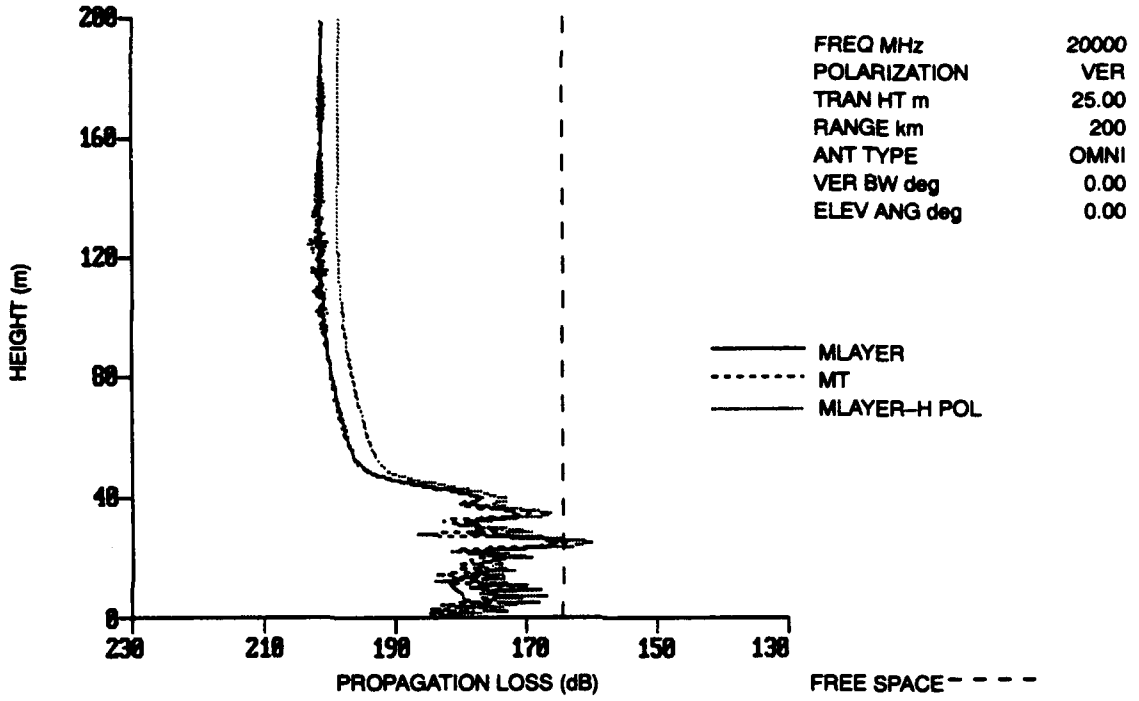


Figure 21. MT vs. MLAYER for smooth surface and vertical polarization, 45.7-meter surface duct, 20 GHz.

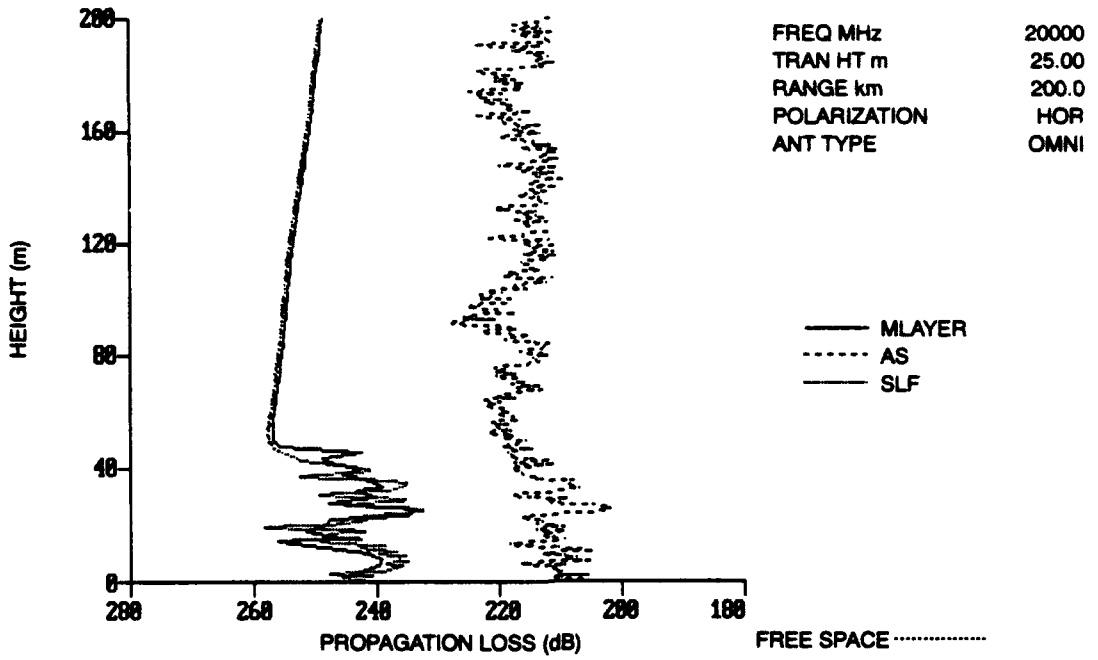


(a)

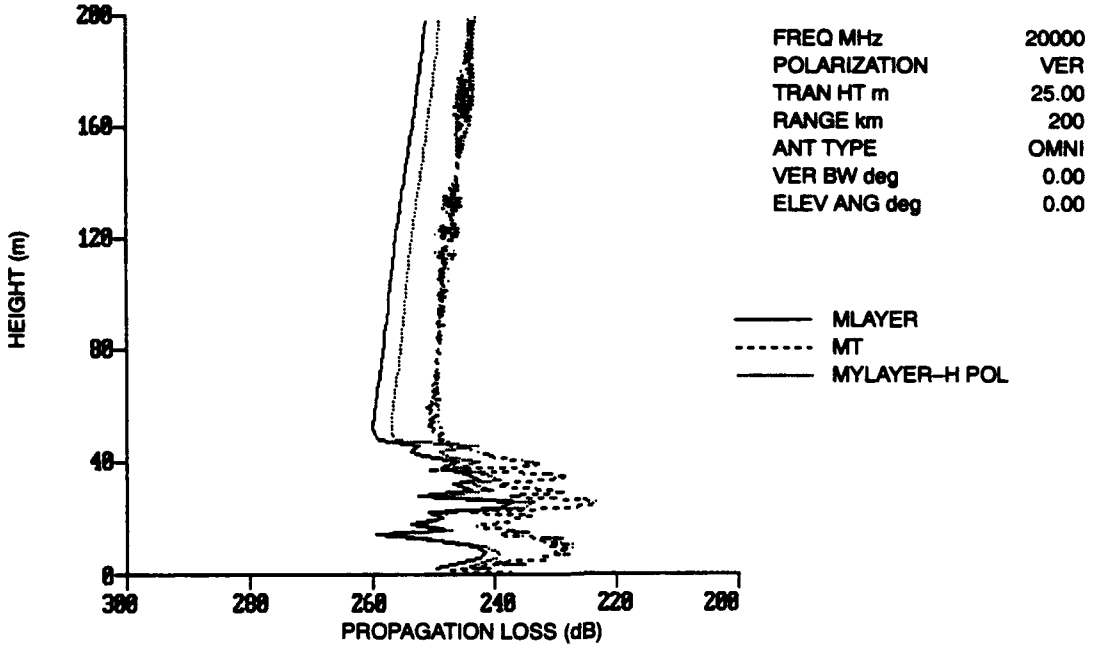


(b)

Figure 22. MLAYER results for 20 GHz, 10-m/s wind speed, 45.7-meter surface duct vs. (a) AS and SLF and (b) MT.

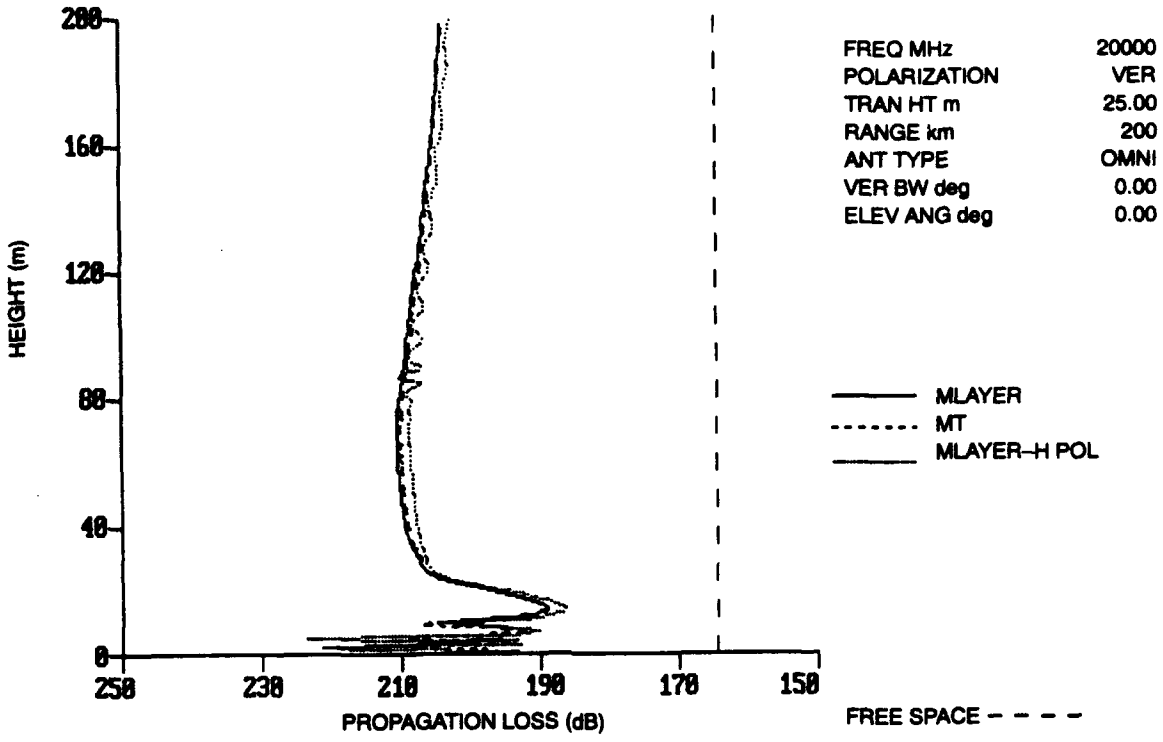


Figure 23. MT vs. MLAYER for smooth surface and vertical polarization, 24-meter surface duct, 20 GHz.

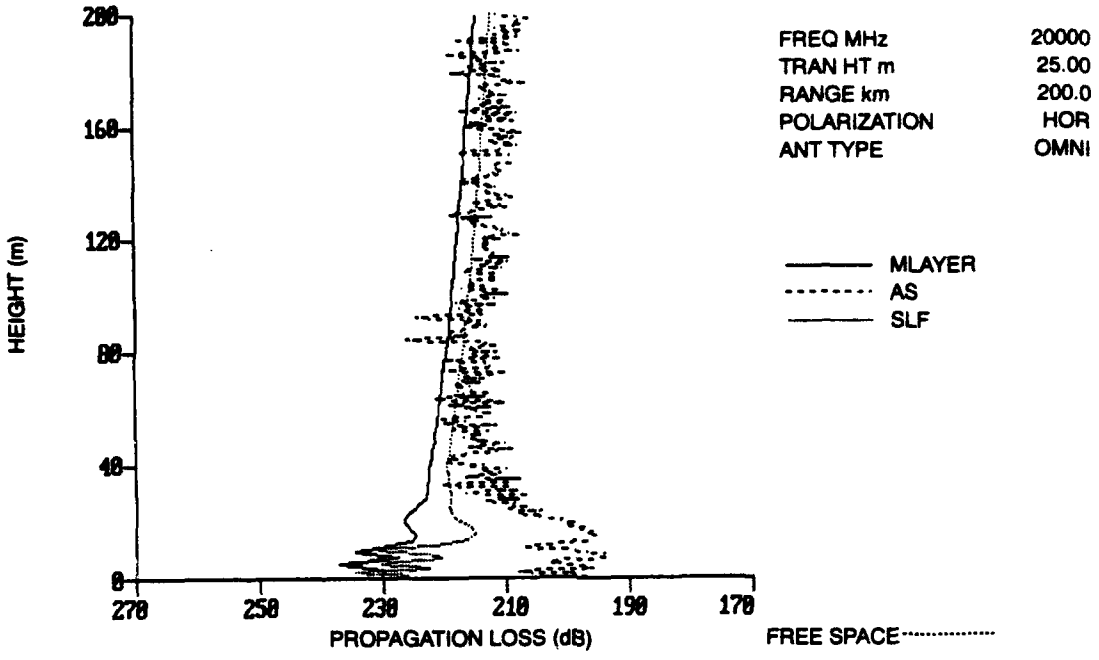


(a)

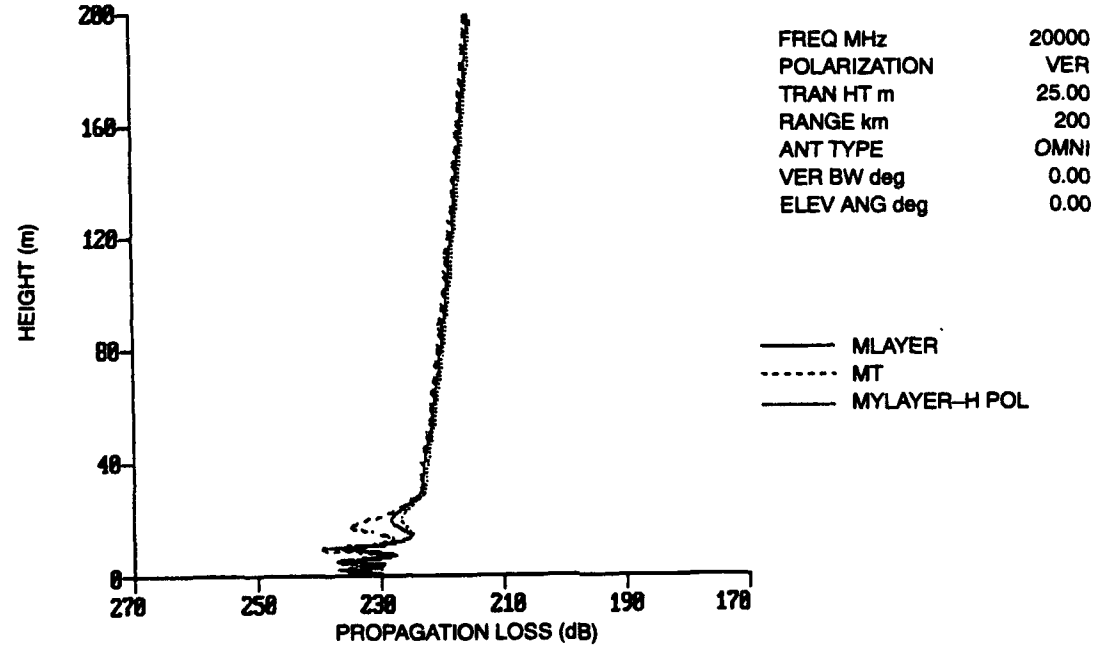


(b)

Figure 24. MLAYER results for 20 GHz, 10-m/s wind speed, 24-meter evaporation duct vs. (a) AS and SLF and (b) MT.

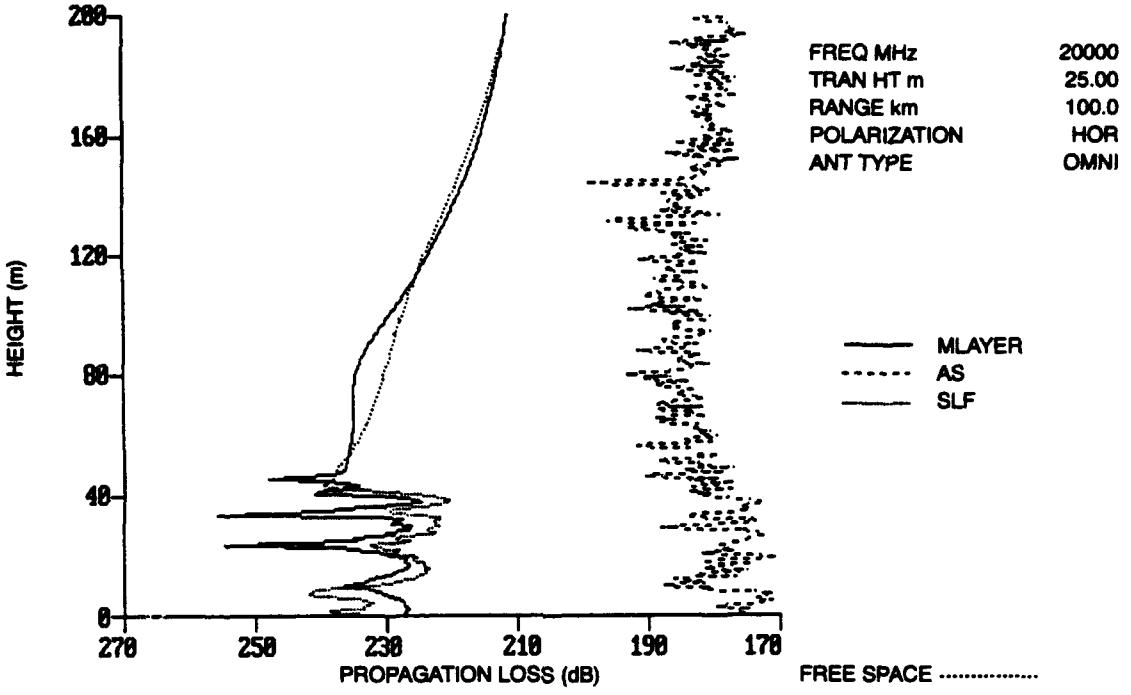


(a)

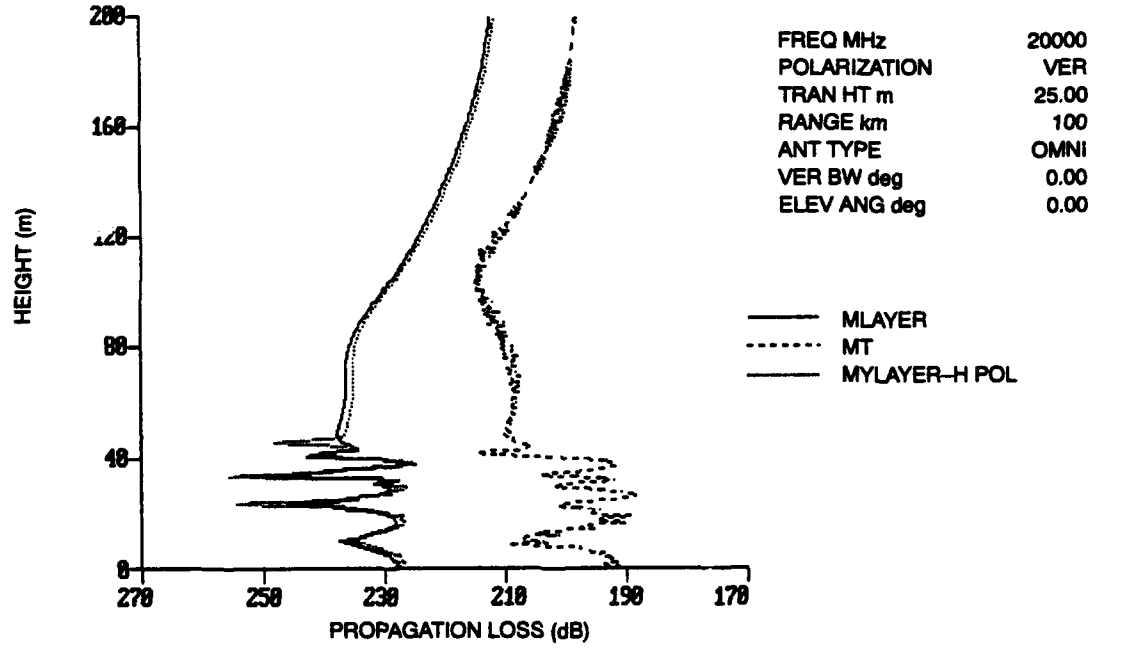


(b)

Figure 25. MLAYER results for 20 GHz, 20-m/s wind speed, 45.7-meter surface duct vs. (a) AS and SLF and (b) MT.

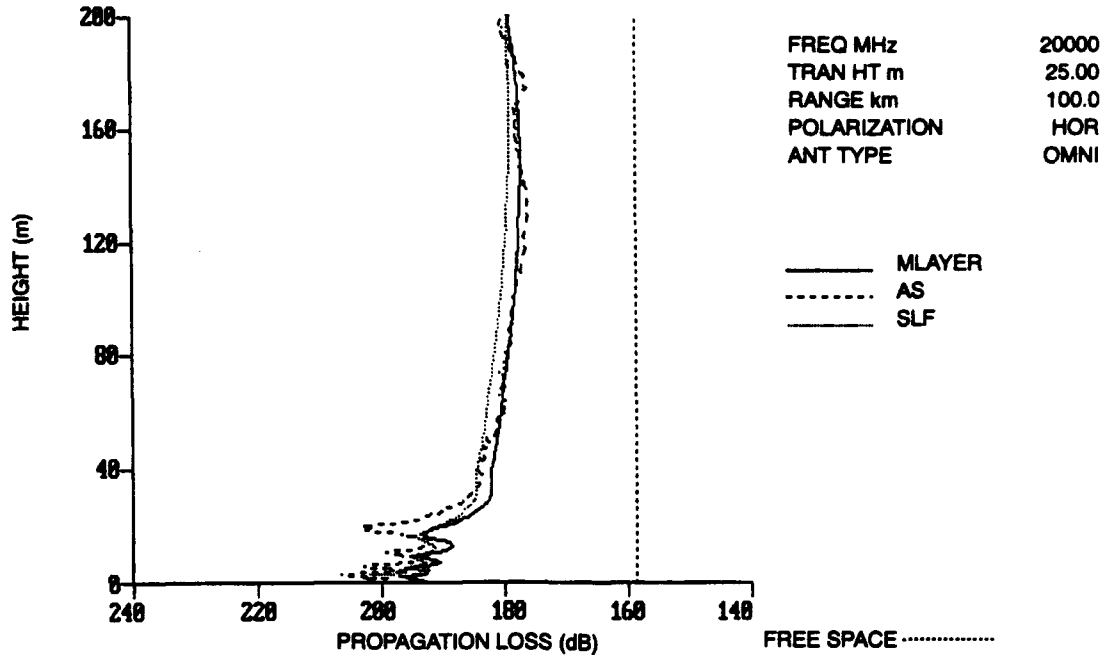


(a)

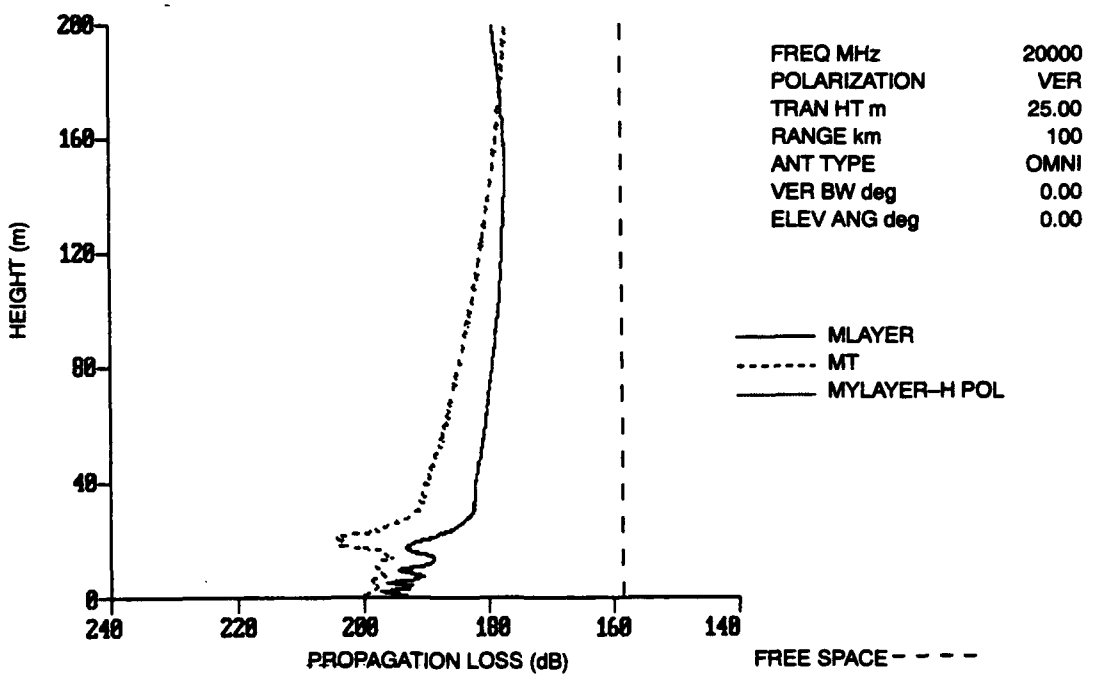


(b)

Figure 26. MLAYER results for 20 GHz, 20-m/s wind speed, 24-meter evaporation duct vs. (a) AS and SLF and (b) MT.

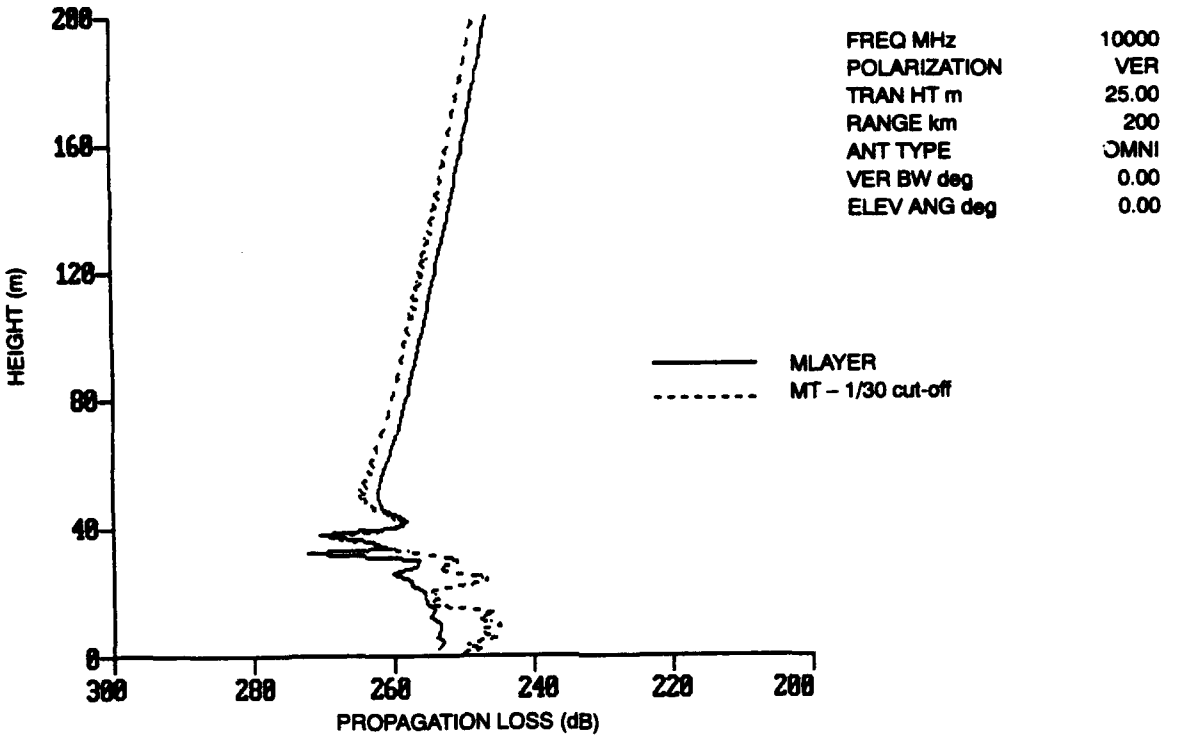


Figure 27. MLAYER vs. MT for 1/30 cut-off. 10 GHz, 45.7-meter surface duct and 20-m/s wind speed.

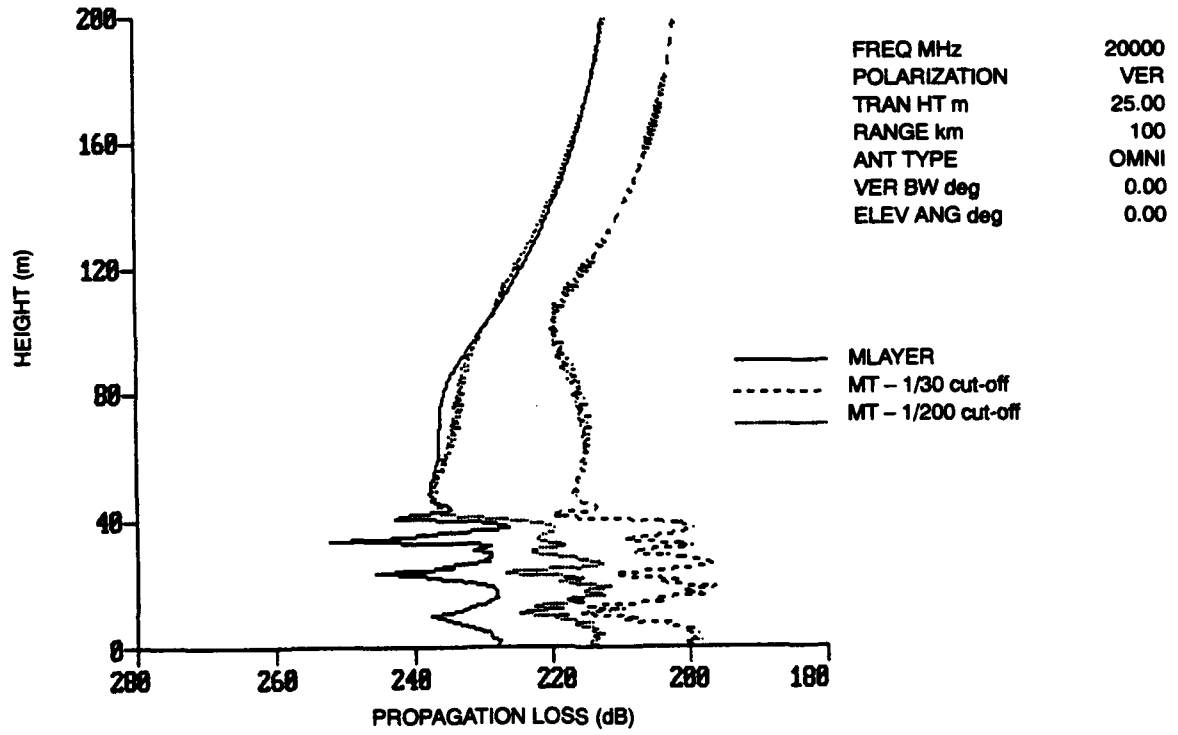


Figure 28. MLAYER vs. MT for 1/30 and 1/200 cut-off. 20 GHz, 45.7-meter surface duct and 20-m/s wind speed.

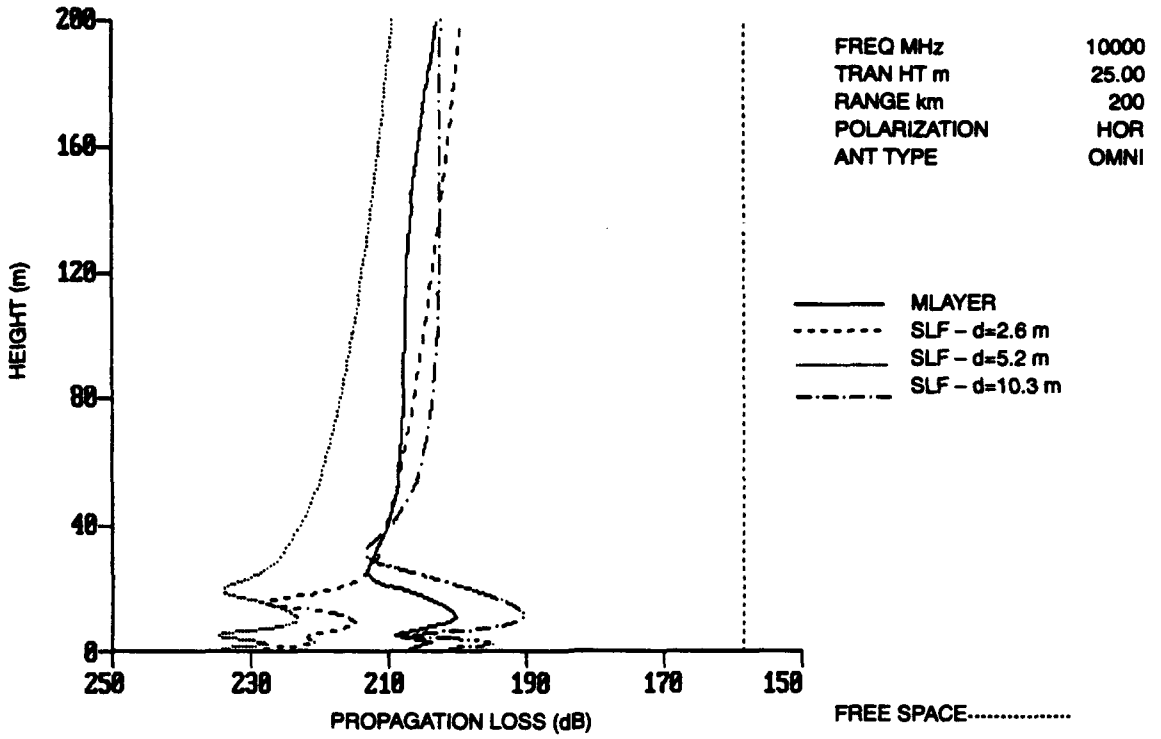


Figure 29. MLAYER vs. SLF for 4-pt ($d$=2.6 m), 8-pt ($d$=5.2 m), and 16-pt ($d$=10.3 m) surface layer heights. 20 GHz, 24-meter evaporation duct and 10-m/s wind speed.

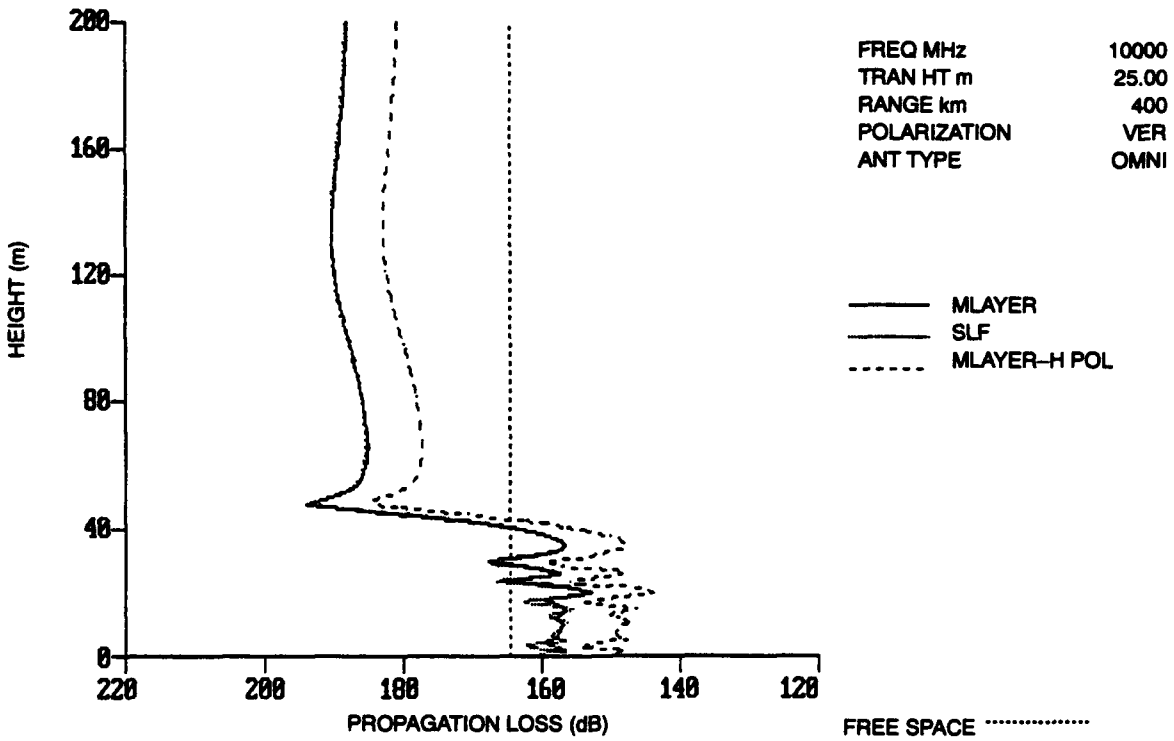


Figure 30. MLAYER vs. SLF for smooth surface, vertical polarization, 45.7-meter surface duct, 10 GHz.

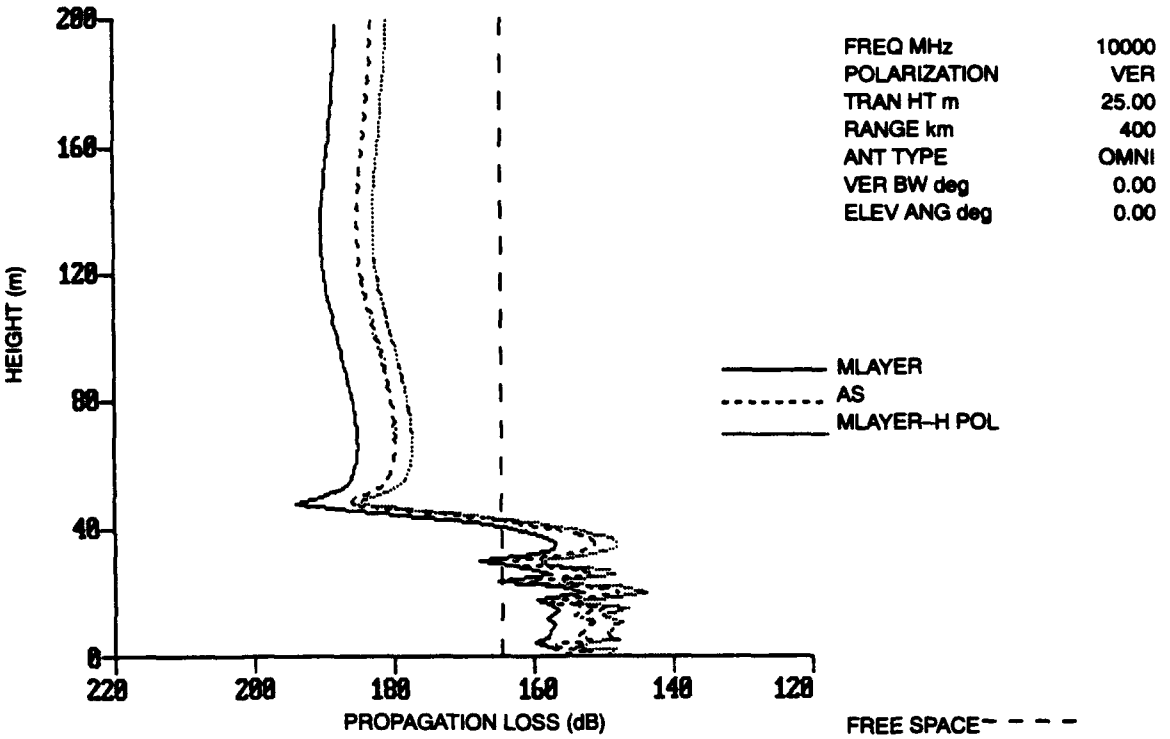


Figure 31. MLAYER vs. AS for smooth surface, vertical polarization, 45.7-meter surface duct, 10 GHz.

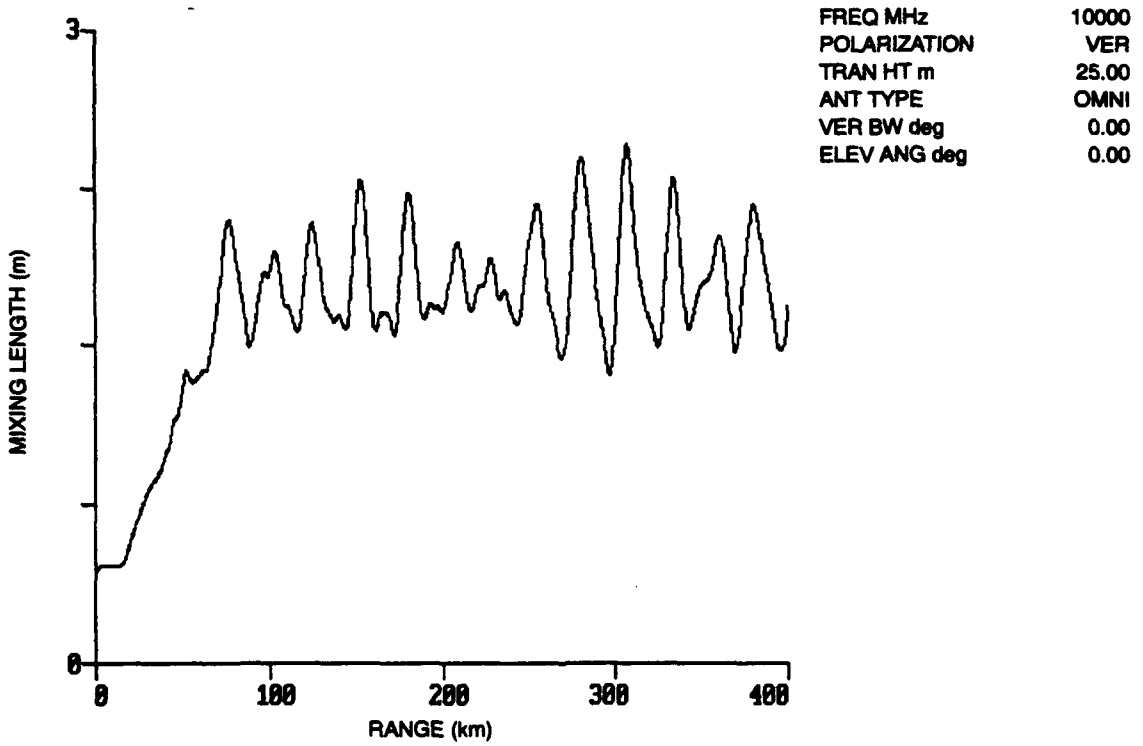


Figure 32. Surface mixing length vs. range for case shown in figure 31.

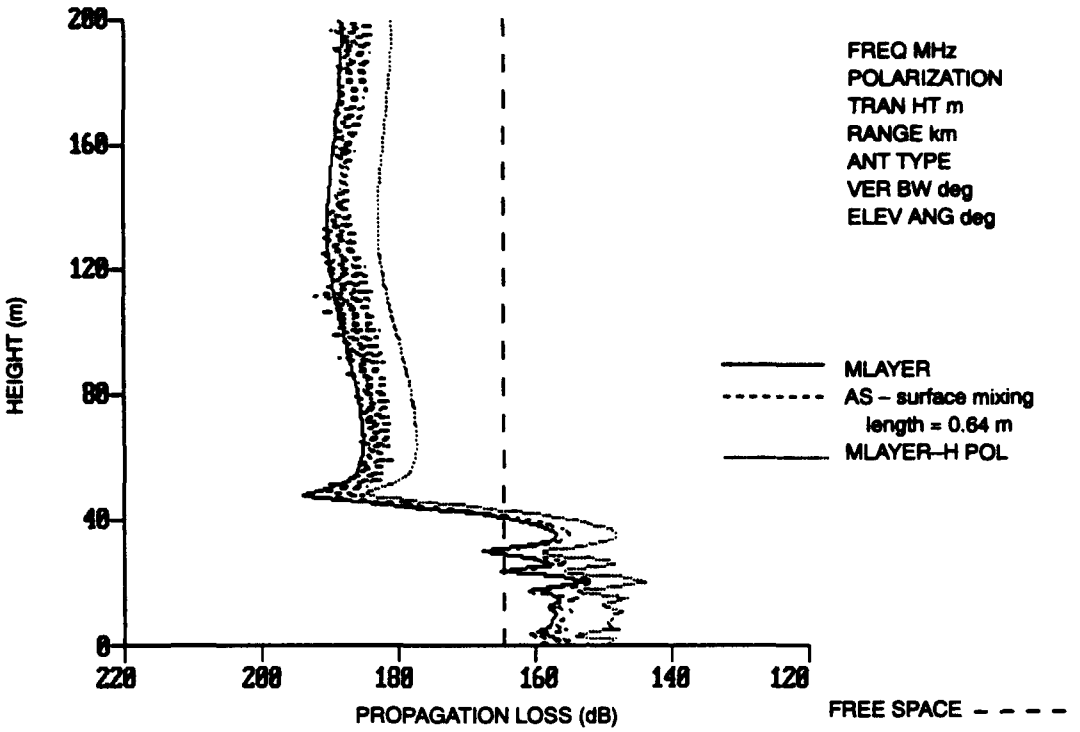


Figure 33. MLAYER vs. AS for case of figure 31 with surface mixing length = 0.64 meters.

# REPORT DOCUMENTATION PAGE

*Form Approved*
*OMB No. 0704-0188*



| 1. AGENCY USE ONLY *(Leave blank)* | 2. REPORT DATE | 3. REPORT TYPE AND DATES COVERED |
|---|---|---|
| | April 1994 | Final; 5/1/93 – 10/31/93 |

**4. TITLE AND SUBTITLE**
ROUGH SURFACE MODELS IMPLEMENTED WITHIN THE SPLIT-STEP PARABOLIC EQUATION ALGORITHM

**5. FUNDING NUMBERS**
PE 0602435N
RO35E81

**6. AUTHOR(S)**
Amalia E. Barrios, Kenneth H. Craig

**7. PERFORMING ORGANIZATION NAME(S) AND ADDRESS(ES)**
Naval Command, Control and Ocean Surveillance Center (NCCOSC)
RDT&E Division
San Diego, CA 92152–5001

**8. PERFORMING ORGANIZATION REPORT NUMBER**
TD 2630

**9. SPONSORING/MONITORING AGENCY NAME(S) AND ADDRESS(ES)**
Office of Naval Research/Code 543
Ballston Tower #1, 800 N. Quincy Street
Arlington, VA 22217–5660

**10. SPONSORING/MONITORING AGENCY REPORT NUMBER**

**11. SUPPLEMENTARY NOTES**

**12a. DISTRIBUTION/AVAILABILITY STATEMENT**
Approved for public release; distribution is unlimited.

**12b. DISTRIBUTION CODE**

**13. ABSTRACT** *(Maximum 200 words)*

Three split-step PE rough surface models—(1) mixed transform (MT), (2) surface loss function (SLF), and (3) approximate solution (AS)—were investigated and compared with a reference waveguide model called MLAYER. The MT and SLF models are shown to agree well with MLAYER; the AS model, however, generally showed poor agreement. The MT model, though the most accurate, is the most time-consuming of the three. The AS model, the most numerically efficient, shows the poorest match to MLAYER.

In using one of these rough surface models, whether it be to model rough surface effects over ocean or variable terrain, a satisfactory compromise may be to use some form of the SLF model since it is shown to agree fairly well with MLAYER and is still fairly efficient.

**14. SUBJECT TERMS**
rough surface models
split-step PE algorithm
radiowave propagation

**15. NUMBER OF PAGES**
50

**16. PRICE CODE**

| 17. SECURITY CLASSIFICATION OF REPORT | 18. SECURITY CLASSIFICATION OF THIS PAGE | 19. SECURITY CLASSIFICATION OF ABSTRACT | 20. LIMITATION OF ABSTRACT |
|---|---|---|---|
| UNCLASSIFIED | UNCLASSIFIED | UNCLASSIFIED | SAME AS REPORT |

| 21a. NAME OF RESPONSIBLE INDIVIDUAL | 21b. TELEPHONE *(Include Area Code)* | 21c. OFFICE SYMBOL |
|---|---|---|
| Amalia E. Barrios | (619) 553-1429 | Code 543 |

# INITIAL DISTRIBUTION (U)

| | | |
|---|---|---|
| Code 0012 | Patent Counsel | (1) |
| Code 0274B | Library | (2) |
| Code 0275 | Archive/Stock | (6) |
| Code 50 | H. O. Porter | (1) |
| Code 54 | J. H. Richter | (1) |
| Code 543 | R. A. Paulus | (1) |
| Code 543 | A. Barrios | (25) |

Defense Technical Information Center
Alexandria, VA 22304–6145 (4)

NCCOSC Washington Liaison Office
Washington, DC 20363–5100

Center for Naval Analyses
Alexandria, VA 22302–0268

Navy Acquisition, Research & Development
Information Center (NARDIC)
Arlington, VA 22244–5114

GIDEP Operations Center
Corona, CA 91718–8000

Office of Naval Research
Arlington, VA 22217–5000 (2)

Space & Naval Warfare Systems Command
Arlington, VA 22245–5200